

**Sofia University "St. Kliment Ohridski"**  
**Faculty of Chemistry and Pharmacy**

**MOLECULAR MODELLING OF PHASE  
TRANSITIONS AT THE WATER-ALKANE  
INTERFACE: ROLE OF SURFACTANTS AND  
CURVATURE**

**Stoyan Iliyanov Iliev**

**A B S T R A C T**

of the PhD thesis submitted for obtaining a degree in  
4.2. Chemical sciences  
(Theoretical Chemistry - Computational Chemistry)

**Thesis supervisors:** Prof. Dr. Anela Ivanova

Acad. Prof. DSc Nikolai Denkov

Sofia, 2024

The thesis was discussed and directed for defence by the departmental council of the Department of Physical chemistry of the Faculty of Chemistry and Pharmacy of Sofia University "St. Kliment Ohridski" held on 02. 09. 2024.

The thesis is written on 114 pages, contains 62 figures, 49 equations and 17 tables in 4 chapters, conclusions, contributions and references. The bibliography comprises 72 titles.

The numbering of figures and tables in the synopsis corresponds to that in the thesis.

*Obtaining and dissemination of the results is funded by the Bulgarian Ministry of Education and Science under the national scientific program "VIHREN", project ROTA-Active (No. KP-06-DV-4/16.12.2019). Computing time for the simulations was provided on the supercomputer Piz-Daint, CSCS, Zurich, Switzerland under the PRACE ICEI projects icp009, icp015 and ch13. Part of the calculations were performed on the supercomputer JURECA, Jülich, Germany under the project EUSMI25.*

## Contents

1.	Introduction .....	3
2.	Literature review.....	4
2.1.	Experimental studies of n-alkanes .....	4
2.1.1.	Structure and properties of n-alkanes in the liquid phase .....	4
2.1.2.	Germ formation and crystal growth.....	5
2.1.3.	Rotator phases in alkane systems .....	7
2.1.4.	Crystal phases in alkane systems .....	9
2.2.	Theoretical studies of n-alkanes .....	10
3.	Computational methods .....	12
4.	Results and discussion .....	12
4.1.	Model systems and computational protocol .....	13
4.2.	Methods for phase state analysis of polycrystallite structures of quasilinear molecules .....	15
4.3.	Identification and separation of the different crystallites in the system .....	16
4.4.	Recovering the real coordinates of molecules in a crystallite.....	18
4.5.	Determination of the crystallite plane and calculation of $\theta$ .....	19
4.6.	Preparation of crystallite for 2D Voronoi tessellation analysis .....	21
4.7.	Calculation of the orientation of the molecules relative to each other.....	22
4.8.	Validation of the used force field .....	24
4.9.	Analysis of physicochemical properties - temperature, enthalpy and density .....	25
4.10.	Germline analysis.....	27
4.11.	Structural analysis of solid phases .....	29
3.11.1.	Overall structuring of frozen systems.....	29
3.11.2.	Local arrangement of alkyl chains in crystallites .....	33
3.11.3.	Crow analysis .....	34
3.11.4.	Rotational order in crystallites.....	35
4.12.	Determination of the type of solid phases obtained at different cooling rates .....	37
3.12.1.	Systems analysed.....	37
3.12.2.	Analysis of enthalpy and mass density of model systems .....	38
3.12.3.	Ratio of gauche/trans conformations in crystallites.....	39
3.12.4.	Analysis of radial distribution functions of crystallites .....	40
3.12.5.	Analysis of the rotational freedom of molecules .....	41
3.12.6.	Determination of the phase state of crystallites .....	42
5.	Conclusion .....	47
6.	Contributions .....	50
7.	References .....	52

## 1. Introduction

Solid state systems composed of normal alkanes (n-alkanes) have been the subject of research for a long time.<sup>1-4</sup> They have many useful applications that are of interest to the petroleum and pharmaceutical industries.

In order to control the properties of alkane-containing systems, the thermodynamic and structural characteristics of their supramolecular formulations and the possible phase transitions between them need to be elucidated. A particular feature of alkanes (in the bulk or in mixtures) is that they have the ability to form transient phases between isotropic liquid and crystal, where the molecules are ordered in all three directions as in a crystal but have a rotational degree of freedom along their long axis. Such states are known as "rotator phases".<sup>2</sup> They can be stable or relatively short-lived and emerge at conditions strongly dependent on chain length and hydrocarbon parity.<sup>2</sup> Understanding the process of formation of such rotator phases, as well as their properties at the molecular level, is critical to explore their full application potential.

There are various data in the literature on the structure of alkanes in liquid and crystalline phases, as well as on phase transitions between them.<sup>1-5</sup> Both experimental and theoretical studies are available. The focus of the present work is on the structural and thermodynamic characterisation of alkanes with chain lengths C14 to C24 and in particular hexadecane, which is the subject of study in this thesis. In the solid state, hexadecane is known to be stable in a triclinic crystalline lattice, but a short-lived rotator phase has also been experimentally detected.<sup>5</sup> Knowledge at the micro-level of how this type of transient phase forms, how it affects the properties of the substance, and how it transitions to the final triclinic phase would greatly aid in the formulation of new experiments where control over the behaviour of the system is critical. This type of knowledge can be obtained most effectively through molecular modelling, where a hexadecane model system can be studied in detail at the molecular level. This approach has been used in the thesis.

The aim of the work is to gain deeper understanding of the behaviour of hexadecane after freezing, as this hydrocarbon is often used as an oil phase in various experimental studies. To achieve this, the following objectives for the thesis are formulated:

1. Development of a computational protocol for molecular modelling of the phase transition from isotropic liquid to solid state in hexadecane-containing systems, such that the protocol may be applied to other alkanes as well.
2. Elucidation of the mechanism of the observed liquid-to-solid transition by analysis of thermodynamic and structural characteristics of the systems.
3. Development of a methodology for analysis of the structure of the resulting solid phases.
4. Determination of the type of solid phases (crystalline or rotator).

## 2. Literature overview

### 2.1. Experimental studies on n-alkanes

At the core of the present work are phase transitions from liquid to solid states in alkane-containing systems. The properties (thermodynamic and structural) of the phases in the two physical states are documented in a number of experimental studies. These are reviewed in the present section. For modelling liquid-to-solid transitions, knowledge of how the ordered phase forms is also required. Therefore, the theory of nucleation during crystallization is also described in detail.

#### 2.1.1. Structure and properties of n-alkanes in the liquid phase

Dymond & Harris study with NMR spectroscopy the diffusion coefficient and density of n-hexadecane at different temperature and pressure.<sup>4</sup> Values of these characteristics at 298 K, 323 K and 348 K are obtained from the experiment and are summarized in Table 1. As expected, as the temperature increases, the alkane density decreases, and the molecules diffuse more easily.

**Table 1:** Diffusion coefficient ( $D$ ) and density ( $\rho$ ) of n-hexadecane at different temperature and ambient pressure.<sup>4</sup>

T [K]	$\rho$ [kg/m <sup>3</sup> ]	$D \cdot 10^{-9}$ [m <sup>2</sup> /s]
298	770	0.38
323	753	0.63
348	736	1.00

In another study, a direct correlation is shown between the free volume of the molecule (alkane), and the fluidity, whereof it is concluded that an intermolecular orientation of the hydrocarbons is already present in the liquid before the phase transition takes place.<sup>1,6</sup>

An important property of normal alkanes is that they can undergo supercooling, which is more pronounced in the odd representatives of the homologous series. A study of the effect of chain length on the homogeneous crystallization of n-alkanes shows that the supercooling effect weakens with chain length extension.<sup>1,7,8</sup> This is most likely due to the relatively structured liquid in these longer alkanes, which allows them to crystallize more readily, and the domains present in the liquid are those that serve as nuclei in the crystallization. At chain length  $\geq C16$  the degree of supercooling ceases to depend on parity.

### 2.1.2. Nucleation and crystal growth

The transition of a system from a liquid to a solid phase requires the formation of a nucleus. In order to understand this process, several theories have been developed and the information about them is summarized by Mura & Ding.<sup>9</sup>

Two theories of nucleation are derived with a phenomenological approach. The first one is based on thermodynamic and kinetic analysis and is called classical.<sup>9</sup> This is the theory used to describe phase transitions in alkanes. The second theory, developed subsequently, assumes that a local increase in density causes the arrangement of a microscopic structure, which then becomes the initial site for crystal formation.<sup>9</sup>

#### 2.1.2.1. Classical theory of nucleation

For a one-component system, nucleation can be divided into two types: 1. Homogeneous, when the nucleus is formed at a random site, and 2. Heterogeneous, when the process is due to interaction with surfaces of different material or impurities.

#### Homogeneous nucleation

To characterize homogeneous nucleation, the system is considered both in terms of its kinetics and with the methods of statistical thermodynamics. In the former case, exchange of single molecules to and from the cluster in the new phase is described, and in the latter the change in energy upon nucleation is calculated.

The kinetic approach is based on two basic assumptions: 1. Initially, the new phase composed of a small number of ordered molecules is confined in a small space, and it is assumed that there is no interaction between adjacent nuclei, and 2. The evolution of the cluster is time-dependent, i.e. the state of the cluster determines the exchange of monomers to and from it.

The formation of a nucleus is associated with release of energy that causes local temperature increase around the cluster (eq. 4).

$$W_n = 4\pi R^2 \sigma - \frac{4\pi R^3}{3v_0} k_b T \ln S \quad (4)$$

$v_0$  denotes the volume of a single molecule in the cluster,  $k_b$  is the Boltzmann constant,  $S$  is the entropy,  $R$  is the universal gas constant, and  $\sigma$  is the surface energy of the nucleus.

In cases where the size of the nucleus is negligibly small compared to the total volume of the system, this does not have a major impact. However, if the system is small, micro or nano sized, the change in temperature is significant. Therefore, in these cases, greater supercooling is required to achieve the crystalline phase.

### Heterogeneous nucleation

In heterogeneous nucleation, the cluster is formed in the presence of another surface type such as substrate or impurity. The shape of the cluster can be described as spherical with a contact angle  $\theta$  that ranges from  $0^\circ$  (complete wetting) to  $180^\circ$  (no wetting; analogous to homogeneous nucleation of an isolated spherical cluster). Young's equation gives the relationship between the contact angle and the specific surface energies of substrate/old phase ( $\sigma_s$ ) and substrate/new phase ( $\sigma_{cs}$ ):

$$\cos \theta = \frac{\sigma_s - \sigma_{cs}}{\sigma} \quad (7)$$

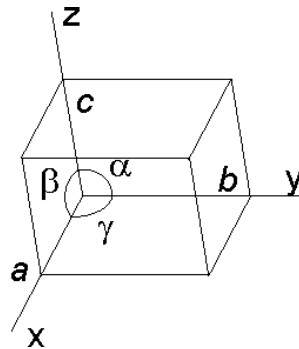
If the nucleus is disc-shaped, the thickness of the disc is fixed and it can only grow in the other two dimensions. Regardless of the shape of the nucleus, the work expressed in equation (4) will be scaled by a factor  $F(\theta)$  that ranges from 0 to 1:

$$F(\theta) = \frac{(1 - \cos\theta)^2(2 + \cos\theta)}{4} \quad (8)$$

When  $F(\theta) \rightarrow 1$  ( $180^\circ$ ) the energy for nucleation will be equal to that of homogeneous nucleation, and when  $F(\theta) \rightarrow 0$  ( $0^\circ$ ) it will be 0. For values between 0 and 1, nucleation will occur close to the substrate due to lower activation energy.

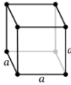
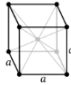
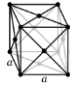
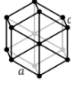
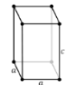
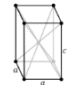
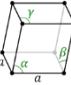
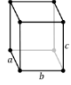
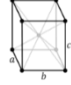
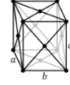
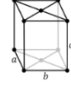
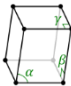
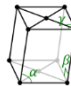
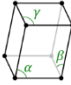
The classical theory provides a good description of the nucleation and crystal growth process of alkanes. This applies to both homogeneous and heterogeneous crystallization.

Once the necessary conditions for nucleation have been achieved, the process of crystallization takes place. Therein, different crystal structures are formed, which can be described by the standard crystallographic syngonies (Table 2). The parameters used to define the lattices are illustrated in Figure 4.



**Figure 4:** Parameters used to characterize a crystal lattice:  $a$ ,  $b$ ,  $c$  denote the translational vectors of the unit cell and  $\alpha$ ,  $\beta$ ,  $\gamma$  denote the characteristic angles.

**Table 2:** Possible lattices and crystallographic syngonies, some of which are observed in the rotator phases of alkanes (see below).<sup>10</sup>

Crystallographic syngony	Lattice parameters	Primitive (P)	Body-centred (I)	Face-centred (F)	Base-centred (B)
<b>Cubic</b>	$a = b = c$ $\alpha = \beta = \gamma = 90^\circ$				
<b>Hexagonal</b>	$a = b \neq c$ $\alpha = \beta = 90^\circ \gamma = 120^\circ$				
<b>Tetragonal</b>	$a = b \neq c$ $\alpha = \beta = \gamma = 90^\circ$				
<b>Rhombohedral (trigonal)</b>	$a = b = c$ $\alpha = \beta = \gamma < 120^\circ$				
<b>Orthorhombic</b>	$a \neq b \neq c$ $\alpha = \beta = \gamma = 90^\circ$				
<b>Monoclinic</b>	$a \neq b \neq c$ $\beta = \gamma = 90^\circ \alpha \neq 90^\circ$				
<b>Triclinic</b>	$a \neq b \neq c$ $\alpha \neq \beta \neq \gamma$				

### 2.1.3. Rotator phases in alkane systems

During phase transitions between liquid and crystalline states in alkane-containing systems, an intermediate phase between the isotropic liquid and the ordered crystalline phase, called rotator phase, is observed. It is characterized by long-range order along all three dimensions of space but has a rotational degree of freedom along the long molecular axis. In alkanes, five different types of rotator phases are known (Figures 5, 6).<sup>2,5</sup>

They can be uniquely characterized by the following four parameters:

**D** - order parameter that determines the degree of deformation of the hexagonal unit cell (Figure 5 a, b). It is defined as  $D = 1 - A/B$ , where A and B are the lengths of the semi-axes (major and minor, respectively) of the ellipse spanning all first neighbors of a given molecule. The parameters of the ellipse are determined by the location of the six nearest neighbors of the molecules in a given crystal layer. In a regular hexagonal lattice A and B are equal and the parameter  $D = 0$ .



$\Phi_d$  - azimuthal angle, which indicates the direction of offset of the nearest neighbours from the long semi-axis of the ellipse (Figure 5b). When the semi-major axis is pointing towards the nearest neighbours,  $\Phi_d = 0$ .

$\theta$  - a measure of the tilt angle of the molecules relative to the plane of the layer in which they are located (Figure 5c).

$\Phi_t$  - angle, which is related to the direction of tilting of the molecules. If in a hexagonal lattice the direction of inclination of the molecules is between their nearest neighbours  $\Phi_t = 0$ , and if it is towards their nearest neighbours  $\Phi_t > 0$  (Figure 6). A non-zero angle  $\Phi_t$  with respect to the semi-minor axis A corresponds to a rotation of the plane in which the molecules are tilted about the c-axis of the crystal.

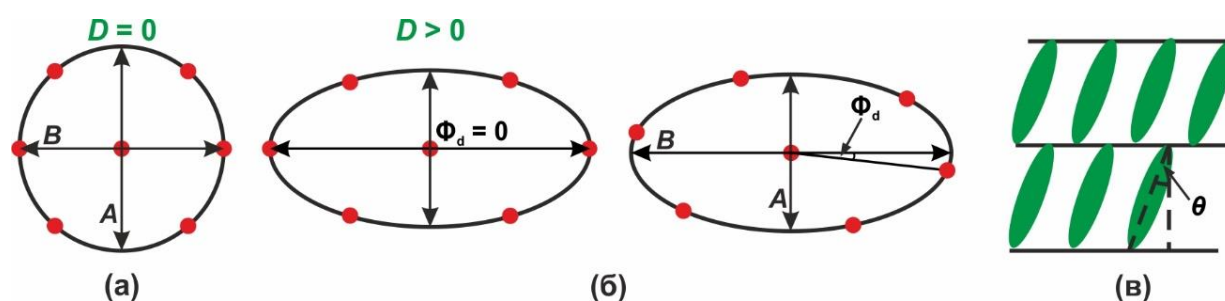


**Figure 5:** Schematic representation of (a) degree of deformation  $D$  and (b) azimuthal angle of a deformed hexagonal lattice; in the left figure  $\Phi_d = 0$ , in the right figure  $\Phi_d > 0$ ; (c) tilt angle of the molecules with respect to the layer plane,  $\theta$ .<sup>2,5</sup>

The differences between all rotator phases known to date with respect to the four structural parameters are shown in Figure 6. Quantitative characteristics of these parameters for the rotator phases, the type of lattice in which the molecules are arranged, and which alkanes exhibit each type of rotator phase are presented in Table 3.

**Table 3:** Structural characteristics of the rotator phases, type of crystal lattice, crystallographic syngony in which the molecules are arranged, and representatives of the alkanes in which the corresponding rotator phase is observed.<sup>10</sup>

Phase	$D$	$\Phi_d$	$\theta$	$\Phi_t$	Structuring of the layers	Lattice in which the molecules are arranged	Number of C atoms
$R_I$	large	0	0	-	ABABAB...	face-centred orthorhombic	$n \leq 25$
$R_{II}$	0	-	0	-	ABCABC...	rhombohedral	$22 \leq n \leq 26$
$R_{III}$	small	$> 0$	$> 0$	$> 0$	AAA...	triclinic	$n \geq 27$
$R_{IV}$	small	0	$> 0$	0	AAA...	monoclinic	$26 \leq n \leq 30$
$R_V$	large	0	$> 0$	0	ABABAB...	face-centred cubic	$23 \leq n \leq 27$

The  $R_I$  phase is characterized by a deformed hexagonal lattice, a face-centred orthorhombic unit cell (Table 2) with  $D > 0$  and the molecules are aligned along the  $c$  axis, i.e.,  $\theta = 0$ . A two-layer arrangement is observed (ABAB...). In  $R_{II}$  the molecules are also upright, but the lattice is not deformed. The arrangement is rhombohedral, and a three-layer sequence takes place (ABCABC...). This phase has the highest symmetry of the five known rotator phases. In  $R_{III}$  the molecules are tilted at an angle  $\theta$  to the plane of the layer in which they are located. The direction of tilt of the molecules is toward the nearest neighbours, i.e.,  $\Phi_t > 0$ . The lattice is slightly deformed and  $\Phi_d > 0$ . The molecules are arranged in a triclinic lattice and a single layer arrangement is observed (AAA...). The  $R_{IV}$  phase is similar to  $R_{III}$ , but the tilt direction of the molecules is toward the second nearest neighbours, i.e.  $\Phi_t = 0$  and the semi-major axis of the ellipse obtained from the deformation of the hexagonal lattice points toward the nearest neighbours, i.e.  $\Phi_d = 0$ . The molecules are arranged in a monoclinic lattice and a single layer arrangement is observed. Similar to  $R_I$ , a strong deformation of the hexagonal lattice is operative in  $R_V$ , with the molecules arranged in a face-centred cubic unit cell. They are tilted between the nearest neighbours and the azimuthal angle  $\Phi_d = 0$ . A two-layer arrangement (ABAB...) follows.

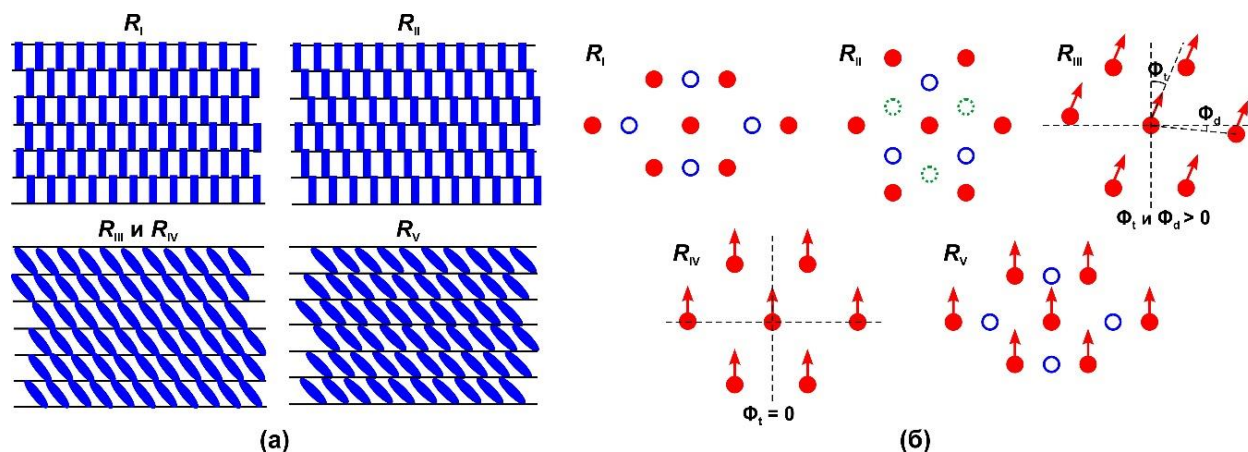


**Figure 6:** Orientation of molecules in different types of rotator phases: (a) orientation in the direction parallel to the longest axis of the molecules. The tilt of the molecules with respect to the plane of the layers and the arrangement of the layers are shown. (b) View in the direction perpendicular to the longest axis of the molecules. The empty blue symbols indicate the molecules of the additional layer of the two-layer structures ( $R_I$  and  $R_V$ ). The molecules of the third layer of the three-layer structure of  $R_{II}$  are marked with empty green dotted symbols. The arrows indicate the direction of the tilting orientation for the structures in which the molecules are at a certain angle.<sup>5</sup>

#### 2.1.4. Crystal phases in alkane systems

The n-alkanes can form various crystal structures with triclinic, monoclinic, orthorhombic, or hexagonal symmetry (Table 2).<sup>1</sup> The molecules are maximally elongated, i.e. all C-C-C-C dihedral angles are in *trans* conformation, and are tightly packed. The symmetry and type of the

crystal lattice are determined by the chemical structure (chain length and parity) of the alkane and by temperature. Nonadecane has an O $\perp$  lattice at 20 °C and a nearly hexagonal lattice at 25 °C. Octadecane, on the other hand, has a triclinic crystal lattice at 20 °C.

In the triclinic crystals of even alkanes, the  $a$  and  $b$  distances are approximately the same from C12 upward, and the magnitude of  $c$  is determined by the length of the alkane. The angles  $\alpha$  and  $\beta$  change slightly with increasing number of carbon atoms (78° - 85° for  $\alpha$  and 62° - 68° for  $\beta$ ), while  $\gamma$  is nearly constant (73°-75°). In the triclinic crystal lattice of hexadecane, the molecules are tilted by 19.4° with respect to the plane of the corresponding layer. The distance between the layers along the  $z$  axis (which coincides with the  $c$  axis when the molecules are not tilted) is 20.6 Å. The crystalline phase is formed at temperature of 16.51 °C.<sup>3</sup> The odd alkanes between C11 and C29 form an O $\perp$  lattice.

The transition from crystalline to rotator phase and then to liquid, unordered phase is characterized by a series of first order phase transitions. There are also transitions between and from different rotator phases, which may be of first or second order.

## 2.2. Theoretical studies of n-alkanes

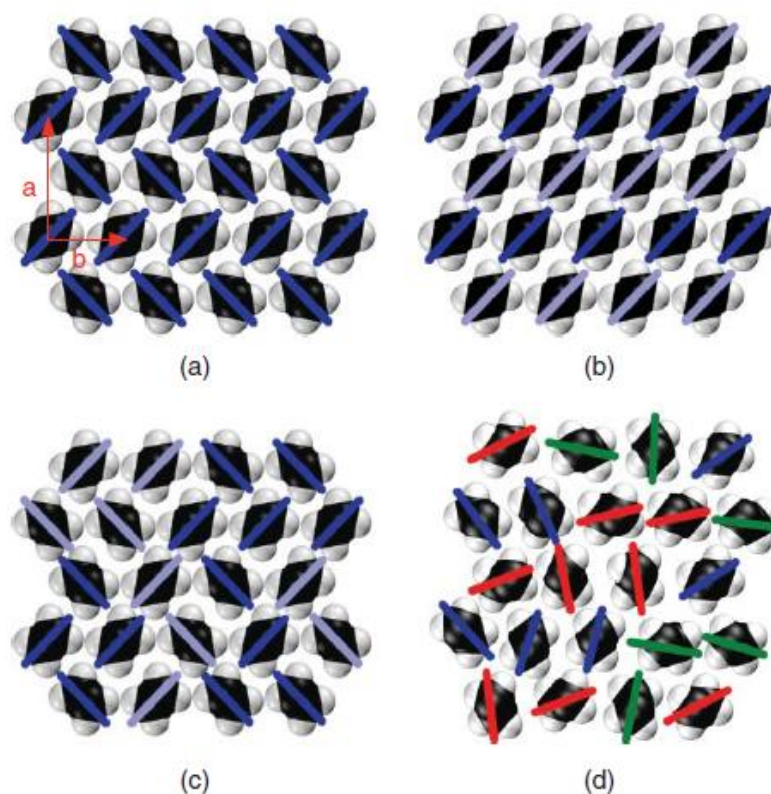
Wentzel & Milner investigate the transitions from the crystalline phase of C23 to the rotator R<sub>I</sub> and from R<sub>I</sub> to R<sub>II</sub>.<sup>11</sup> The MD simulations are performed in N $\sigma$ T ensemble where the number of particles, the stress tensor and the temperature are constant. The used force field is Flexible Williams (FW).<sup>12</sup>

Figure 15 presents the solid phase structures of C23. Local order parameters are defined that vary for the four observed phases (orthorhombic crystalline, monoclinic crystalline, R<sub>I</sub> and R<sub>II</sub> rotator). The first one is the Potts order parameter ( $q = 0, 1, 2$ ). Each value of  $q$  determines the orientation of the layer of molecules along one of the principal axes of the crystal lattice. The second one is the Ising order parameter ( $s = 0, 1$ ), which describes whether the molecule is rotated at 45° or -45° with respect to the  $a$  axis.

The defined order parameters are monitored for both the heating and cooling simulations. Upon heating, the initial orthorhombic lattice transitions to a monoclinic lattice, then it transforms in R<sub>I</sub> phase and finally R<sub>II</sub> is observed. Upon cooling, however, instead of the expected transition from the R<sub>I</sub> to the orthorhombic phase, a monoclinic one is obtained. The transition temperatures between the different ordered phases are compared with experimental ones (Table 6). A hysteresis is observed in the simulations, which is absent in the experimental studies. This is due to the excessively fast temperature scan rate.

The internal energy change of the system upon heating is also monitored to determine the thermodynamic characteristics of the phase transitions, with a deviation from experiment of ~5 kJ/mol.

An inaccuracy in the simulations is that the monoclinic crystalline phase is more stable than the orthorhombic one, which is inconsistent with experiment. This is due to the chosen force field and the small difference in the energies of the two phases.



**Figure 15:** Types of solid phases of C23 shown in a view perpendicular to the  $ab$  plane. The coloured lines indicate the orientation of the molecules. The colour of the lines indicates the arrangement of the molecules (Ising - light- or dark-blue, Potts - red/green/blue): (a) orthorhombic crystal lattice with herringbone orientation (b) monoclinic lattice (c) orthorhombic  $R_I$  phase (d) hexagonal  $R_{II}$  phase.

**Table 6:** Phase transition temperatures for C23 upon heating and cooling. The left column denotes the temperatures obtained from simulations and the right column – from experiment.

	Simulation		Experiment	
	Heating (K)	Cooling (K)	Heating (K)	Cooling (K)
Crystal - $R_I$	317	300	313.32	312.01
$R_I$ - $R_{II}$	336	327	317.90	317.90

Marbeuf & Brown conducted MD simulations of C18, C19 and C20 alkanes at temperatures close to those of melting of the respective hydrocarbon.<sup>13</sup>

In simulations of C19, a spontaneous transition from an orthorhombic crystalline phase to  $R_I$  is observed at 290 K. At temperatures from 285 K upward, correlated "jumps" of molecules along the  $c$  axis with magnitude of  $\pm 1.2$  Å and rotations of molecules by  $90^\circ$  about their long axis are observed. This effect has also been recorded in a previous work and was found to initiate the transition to  $R_I$ .<sup>14</sup>

Two transition phases, pseudo  $R_I$  and pseudo  $R_{II}$ , are observed for the two even alkanes. These are characterized by "jumps" of individual molecules and rotation about their long axis of

90° for R<sub>I</sub> and 60° for R<sub>II</sub>. Unlike C19, here the molecules resume their initial position more rapidly and more closely resemble oscillations about their equilibrium position along the *c* axis.

Burrows et al. compare the accuracy of seven different force fields to describe phase transitions in normal alkanes, which include CHARMM36<sup>15</sup> and L-OPLS<sup>16,17</sup>. The alkanes studied are C8, C15 and C16, with C8 included to check how the estimated properties scale with chain length. The self-diffusion coefficient (*D*) as well as the density of the three alkanes with all force fields at 298 K are obtained. Overall, it can be concluded that none of the force fields reproduces all the studied properties of the two alkanes. However, the reason for this may not be the potentials themselves, but the partial changes that have been made to them which can impair the transferability of the parameters, and also the highly nonequilibrium procedure used in the simulations.

Gamisch et al. develop energy storage materials in the form of a water/C<sub>22</sub>H<sub>45</sub>OH (1-docosanol) emulsion.<sup>18</sup> Model systems of 1-docosanol and 1-docosanol in the presence of a crystalline nucleus of 1-pentacontanol (C<sub>50</sub>H<sub>101</sub>OH) or n-heptacontane (C<sub>70</sub>H<sub>142</sub>) are constructed. The results show a 30 K increase in crystallization temperature for both models with added crystalline nucleus relative to the bulk system without nucleus. The authors do not detect the presence of a rotator phase due to the computational protocol used (large temperature intervals between the production parts and the force field used).

The results described so far are in most cases based on relatively short simulations due to the limitations in the computational resources available at the time of conducting these studies. In some cases, average thermodynamic characteristics are presented where the system is either not yet in equilibrium or, due to the choice of computational protocol, the simulations are conducted at a constant change in system temperature, which is inconsistent with the equilibrium molecular dynamics formulation. Also, model systems of emulsions composed of alkane and surfactants are yet to be studied. Such systems have been shown to undergo a rotator phase transition near the interface, even though the same alkane in bulk does not exhibit such behaviour.<sup>5</sup>

### **3. Computational methods**

The basic principles of the classical molecular dynamics method, which the studies are carried out with, as well as some key structural analyses are described in the thesis.

### **4. Results and discussion**

The chapter presents in the following order the results obtained during the work on the thesis: first, the protocol for building and simulating the models is presented. Then, the developed methodology for structural analysis and determining the phase state of the model systems is detailed. This procedure is validated with comprehensive analyses of both the thermodynamic characteristics and the structural properties of some of the model systems. Finally, the

methodology developed in the thesis is applied to a large set of model systems and their phase state is determined. Conclusions are drawn about the initial preferred phase of the hexadecane-containing systems after freezing. The probable phase transitions for this type of systems from isotropic liquid to triclinic crystal are also presented.

#### 4.1. Model systems and computational protocol

The models investigated in the thesis consist of bulk hexadecane (denoted in the thesis as bulk HEX) and hexadecane on a flat water surface stabilized by two surfactant layers (HEX/Surf/water). The two types of model systems are investigated in order to characterize the phase transitions occurring therein upon cooling from the liquid state. The bulk hexadecane model is composed of 440 molecules or 22000 atoms. The HEX/Surf/water model consists of 494 hexadecane molecules, 108 surfactant  $C_{16}(EO)_2$  molecules, and 2778 water molecules ( $\approx 43000$  atoms total). The surfactant is organized at a flat interface with water in the presence of hexadecane (the HEX/Surfactant ratio is 1:2). The model systems are presented in Figure 18.

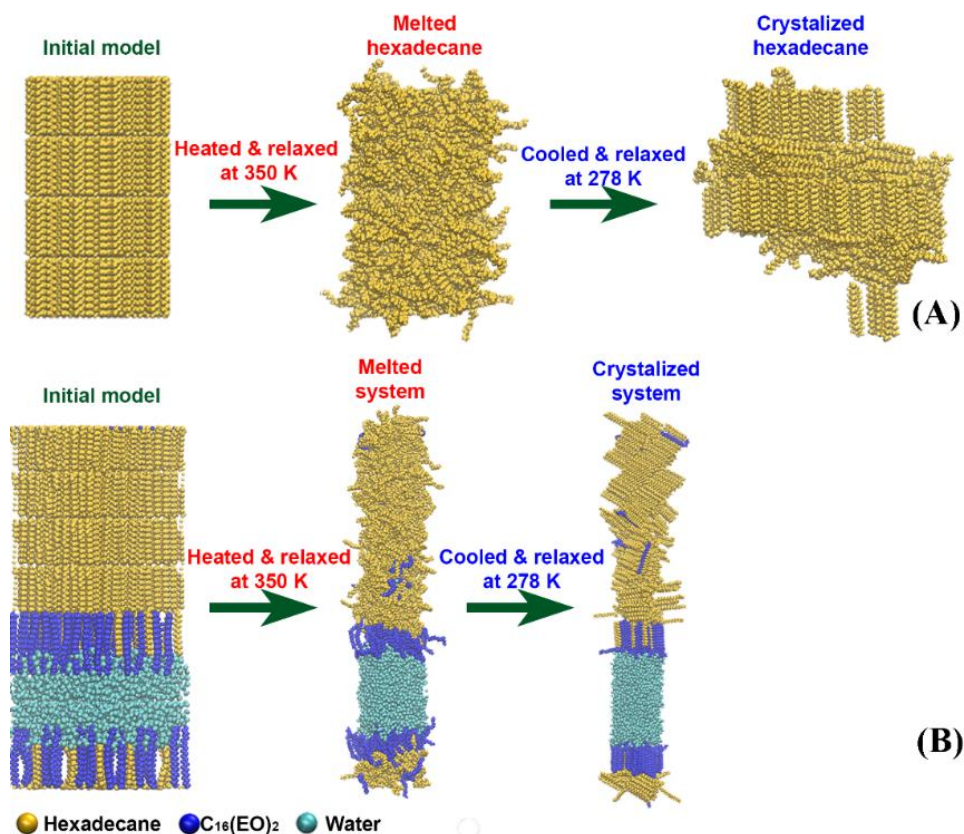


**Figure 18:** Illustration of the simulated molecular models of (A) bulk HEX and (B) HEX/Surf/water.

The initial structures of the two types of models are arranged with the molecules placed at the nodes of a hexagonal lattice and each molecule rotated at a random angle about its long axis in order to accelerate the melting process. The initial area per molecule is  $0.195 \text{ nm}^2$ , which corresponds to the experimental value for hexadecane in a triclinic crystal.<sup>5</sup> The bulk HEX model consists of four layers oriented along the  $c$  axis (collinear with the  $z$  axis of the periodic box). Each layer contains 110 molecules with 11 in each row along the  $x$  axis and 10 in the  $y$  direction. The HEX/Surf/water system has the same hexadecane structure with an added symmetric surfactant/water/surfactant layer (Figure 18). Initially, the surfactant/HEX ratio in the surface monolayer is 1:2, which is consistent with experimental studies.<sup>5</sup> In the course of the simulations, this ratio in the surface layers and in the bulk is free to change. The hydrophilic surfactant heads are hydrated with water molecules from a periodic liquid water box simulated at 300 K.<sup>19</sup> The initial thickness of the aqueous layer is 4.5 nm.

All simulations are carried out in a hexagonal periodic box with initial dimensions of  $5.2 \times 4.5 \times 9 \text{ nm}$  for bulk HEX and  $5.2 \times 4.5 \times 17.2 \text{ nm}$  for HEX/Surf/water. Periodic boundary conditions are applied in all directions.

The systems are first energy-minimized and then heated to 350 K at a rate of 1 K/ps in an NVT ensemble. A simulation of 200 ns is performed in the NPT ensemble ( $P = 1 \text{ bar}$ ) in order to equilibrate after reaching the final temperature. As a result, the systems attain an isotropic liquid phase state, and the last frame is used as the initial frame for subsequent MD simulations of the corresponding model. As a next step, the systems are cooled to 300 K or to 273 K again with a cooling rate of 1 K/ps. Cooling to various temperatures below 300 K is also performed in order to determine the highest simulation temperature at which all systems undergo a phase transition from isotropic liquid to a solid ordered phase. As a result, 278 K is determined as the freezing temperature. All trajectories at the different low temperatures are 200 ns long, except for the systems at 278 K, which are 1000 ns long. In order to investigate the effect of the cooling rate on the process of formation of the ordered phase, the models are cooled to 278 K at four different rates (1 K/ps, 0.1 K/ps, 0.01 K/ps, 0.001 K/ps). For each model system at each cooling rate, three independent trajectories are generated for statistical significance of the outcome. The resulting solid phases are analysed.<sup>20</sup>

The production trajectories are in NPT ensemble with isotropic pressure scaling for bulk HEX and semi-isotropic scaling for HEX/Surf/water. The type of scaling for both types of systems is chosen based on numerous molecular dynamics studies of soft matter from recent decades, e.g., of lipid bilayers solvated in water (for which semi-isotropic scaling is recommended).<sup>15</sup> The chosen thermostat and barostat are  $v$ -rescale<sup>21</sup> with contact time 0.1 ps and Berendsen<sup>22</sup> with contact time 0.8 ps, respectively. The isothermal compressibility in all directions is  $7.3 \times 10^{-5} \text{ bar}^{-1}$ .<sup>23</sup> The Berendsen barostat is chosen because it allows semi-isotropic scaling for HEX/Surf/water systems and is also numerically stable, which is of utmost importance in case of phase transitions. A combination of a Parrinello-Rahman barostat<sup>24</sup> and a Nosé-Hoover thermostat<sup>25</sup> is also tested with the same contact times as the previous pair at 278 K. After 500 ns of simulation, no transition from liquid to solid state is observed.

The Van der Waals interactions are calculated with the Lennard-Jones potential with cut off at 1.2 nm with a switch function activated at 1.0 nm. Electrostatic interactions are evaluated with PME,<sup>26</sup> where the summation of the real part is up to 1.2 nm with a switch function turned on at 1.0 nm. The interpolation of the charges on the lattice in the reciprocal space is done with a fourth order polynomial using the B-spline algorithm. The distance of the nodes along the mesh is 0.12 nm.

The time step is 2 fs, and the equations of motion are integrated with leap-frog. The lengths of all hydrogen-containing bonds in the organic molecules is fixed with LINCS,<sup>27</sup> and that of the bonds in water is constrained with SETTLE.<sup>28</sup> The coordinates are saved in the trajectories every 10 ps.

Four atomistic force fields are tested: CHARMM36,<sup>15</sup> Lipid17,<sup>29</sup> AMBER99<sup>30</sup> and OPLS-AA<sup>16</sup> in combination with TIP4P<sup>19</sup> water model. The force fields are chosen for their parameterization for a large set of lipids with a focus on accurately describing the structuring of the alkyl tails. The initial configuration for the simulations with each of the force fields is identical and the computational protocol is as that described above.

All simulations are carried out with the software package Gromacs 2020.<sup>31</sup> The program VMD 1.9.4 is used to visualize the trajectories.<sup>32</sup>

The last 100 ns of the production stages of all generated trajectories are subjected to statistical analysis.

The procedures and analyses described in Chapters 4.3 to 4.7 are developed in the Python programming language in combination with the MDAnalysis 2.1.0<sup>33</sup> and NumPy 1.22.3 libraries.<sup>34</sup> The main function of MDAnalysis is the translation of MD trajectory data into arrays, allowing the development of complex structural analyses. For the mathematical operations required in the analyses, the NumPy library is used to provide the necessary speed of calculations. Some of the plots are made with the library Matplotlib 3.5.2.<sup>35</sup>

#### **4.2. Methods for analysis of the phase state of polycrystalline structures of quasilinear molecules**

The applied computational approach described above, in which there is no external bias in the arrangement of the molecules, results in more than one crystallite in each of the studied systems (Figure 19). In all cases, there are also still disordered molecules at the end of the molecular dynamics trajectories.

To investigate the phase state of the individual crystallites, a procedure for identifying the molecules in each crystallite and isolating them is required, which is developed as part of the thesis, as are all the data processing methods in this chapter.



### 4.3. Identifying and separating the different crystallites in the system

As shown in Figure 19, the different crystallites in the system are oriented in different directions of space. This property can be used as a criterion to isolate them. To obtain a quantitative measure of this orientation, vectors spanning each HEX molecule and/or surfactant alkyl tail are constructed. Each vector spans the atomic positions from the third (C3) to the fourteenth (C14) carbon atom (Figure 20, A)

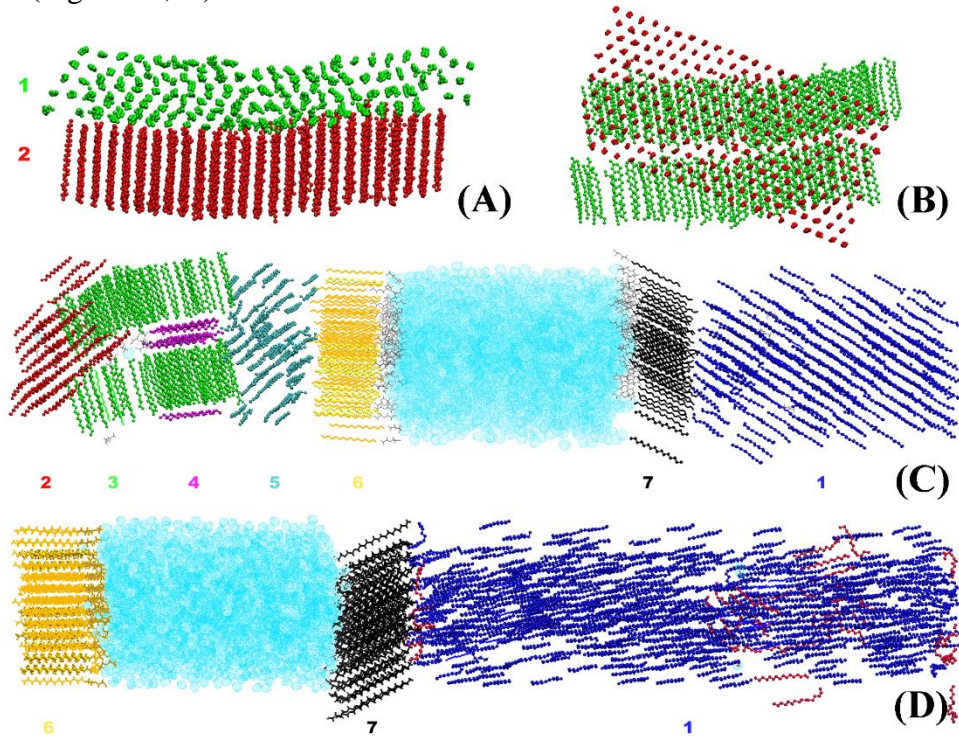


**Figure 19:** Illustration of the polycrystalline structure of the two types of model systems studied in the thesis on frames after 1000 ns of simulation at a cooling rate of 1 K/ps: (A) side view of the crystallites in bulk HEX, (B) top view of the same crystallites, (C) HEX/Surf/water with multiple crystallites, (D) HEX/Surf/water where the hexadecane in the system is arranged in a single crystallite accompanied by disordered hexadecane molecules (coloured in red). Each colour indicates a different crystallite in the corresponding system and all crystallites are numbered. Hexadecane is represented by beads, surfactant tails by bold lines, surfactant heads by thin lines and water by bubbles.

The slopes  $B_{ij}$  of the projections of the  $\overrightarrow{C_3C_{14}}$  vectors of each molecule in the  $xy$ ,  $yz$  and  $zx$  planes of the coordinate system are calculated. The slopes are averaged over a time period where the system is in a steady state, in the case of the systems studied in the thesis these are the last 50 ns of each MD trajectory.

The obtained slopes are then plotted on a 3D graph (Figure 20, B, C, D) where well-separated clusters of points are observed. Each cluster corresponds to one crystallite and is identified numerically by the range of values it spans along the three axes. Points that are not in

close proximity to others belong to molecules that are not in a crystallite, i.e., are in a disordered state. In the case of a perfectly ordered crystal, the orientation of all the molecules therein will be nearly the same. Hence, the cluster of points will appear small or as a single point. In this case, the standard deviations (much smaller than for a disordered molecule) obtained from the time averaging will uniquely identify such crystals (Figure 20, D).

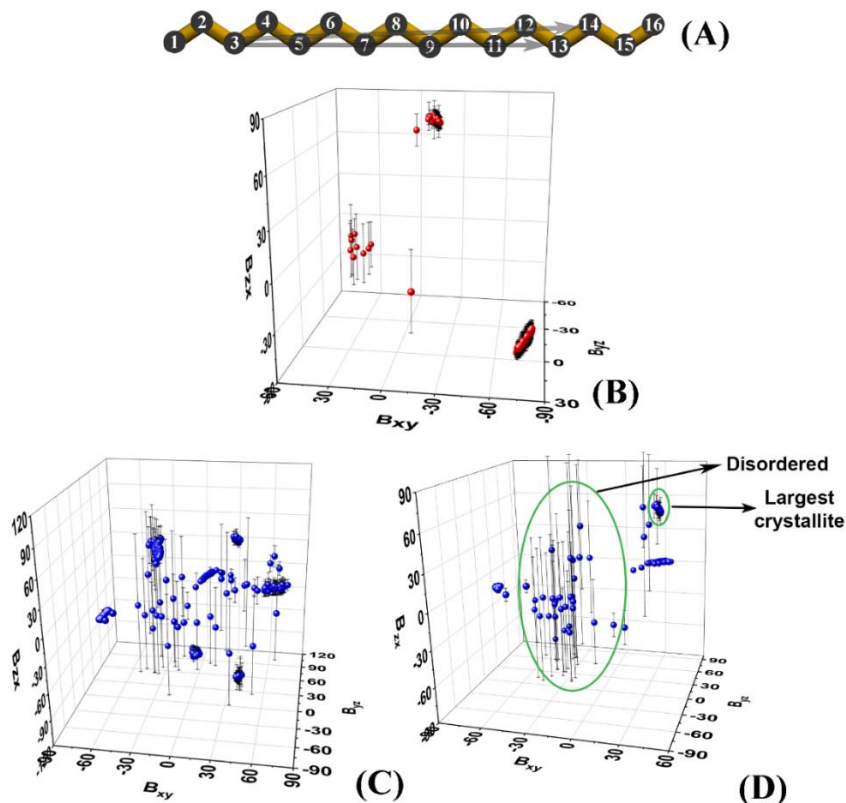


**Figure 20:** (A) Carbon skeleton of HEX with atom numbering; the two arrows show the vectors  $\overrightarrow{C_3C_{13}}$  and  $\overrightarrow{C_3C_{14}}$  that are used in the developed analyses; 3D plots of the slopes of the vectors  $\overrightarrow{C_3C_{14}}$  averaged over the last 50 ns of the MD trajectory in (B) bulk HEX, (C) HEX/Surf/water, and (D) HEX/Surf/water with a single crystallite of bulk HEX

Once the molecules in each crystallite are identified, they can easily be separated. However, the crystallites often appear scattered in the simulation box (Figure 21, A, B) due to the periodicity of the box.

This separation of molecules in the crystallite at different ends of the simulation box makes it impossible to apply much of the analysis described below. Therefore, a procedure is needed to reconstruct the real coordinates of the molecules in the crystallite.

#### 4.4. Reconstructing the real coordinates of the molecules in a crystallite

Crystallites that are separated in the periodic box are characterized by a void between the centre-of-mass (COM) of the molecules in the individual segments (Figure 21, A). The procedure accounts for these empty spaces and measures the distance between the different segments, thereby identifying the molecules in each segment which are to be periodically imaged. The images are obtained by translation along one of the vectors of the periodic box. If images are to be translated in different directions, this is done sequentially. The procedure is illustrated graphically in Figure 21, A.

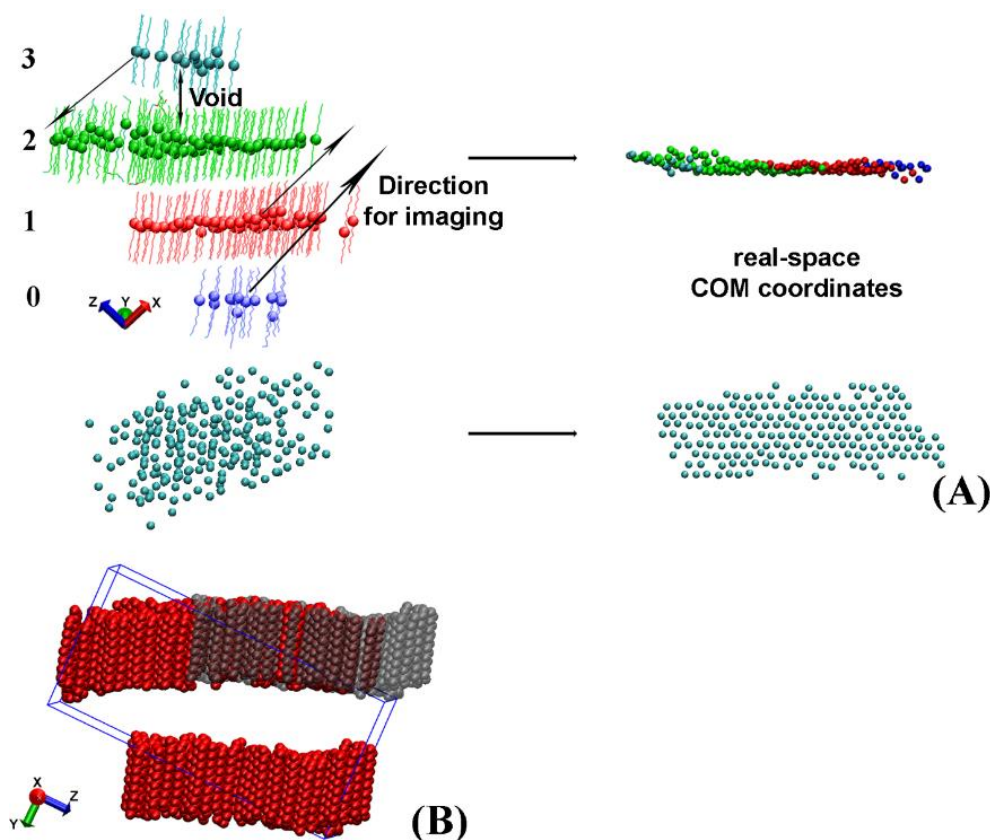


**Figure 21:** (A) Illustration of the procedure to restore the integrity of a crystallite dispersed in the simulation box shown for a HEX/Surf/water system. Each bead represents the COM of a molecule in the crystallite. The numbers on the left of the figure are indices of the different segments of the crystallite. In the example given, the direction in which images of the individual segments are taken is  $\pm x$ . (B) Illustration of a large bulk HEX crystallite that is split in the periodic box in the  $y$  direction. The molecules in red are those conserved in the trajectory, and the gray ones are from the segment of which the periodic image is generated along  $+y$ .

This procedure is executed for each frame of the studied part of the trajectory. It is important to note that the procedure will only work in cases where, by generating periodic images

of individual segments of the crystallite, their number decreases. If the crystallite has a multilayer structure, the procedure will not change it.

The crystallite can then be analysed to determine its phase state. The first structural parameter that is essential for this is the tilt angle of the molecules with respect to the plane of the crystallite,  $\theta$  (Figure 5).

#### 4.5. Determining the crystallite plane and calculating $\theta$

A way to determine the plane of a crystallite is by conducting principal component analysis.<sup>36</sup> This involves calculating a covariance matrix composed of the  $x$ ,  $y$ , and  $z$  coordinates of a mid-chain atom of each molecule in the crystallite. In this case, C8 (Figure 20, A) is chosen for HEX or the tail of a surfactant.

A similar matrix is used by Ryckaert et al.<sup>14</sup> In their work, however, the method only allows the calculation of the average angle of the molecules with respect to the  $z$ -axis of the coordinate system, and not with respect to the local plane of the crystallite. In the thesis, the first three principal components are used to determine the crystallite plane in the manner described below. As a next step, the tilt of the molecules with respect to this plane is calculated.

The eigenvectors of the covariance matrix<sup>37</sup> form an orthogonal basis in which each eigenvector describes a percentage of the variation in the coordinates of the atoms in a given direction of space. The vector with the smallest eigenvalue will describe the smallest variation, which means it will be perpendicular to the plane in which the coordinates of the atoms are arranged. This vector ( $\vec{N}$ ) can be represented in matrix form with its three components  $a$ ,  $b$  and  $c$ :

$$\vec{N} = \begin{bmatrix} a \\ b \\ c \end{bmatrix} \quad (44)$$

With these components one can also construct the parametric equation of the crystallite plane, which has the form:

$$a.x + b.y + c.z = d \quad (45)$$

The free parameter  $d$  is calculated as the scalar product of  $\vec{N}$  with a vector of the averaged  $x$ ,  $y$ , and  $z$  coordinates of the C8 atoms in the crystallite (the average of each row of  $\mathbf{M}$ ). Examples of two planes calculated in this way are shown in Figure 22.

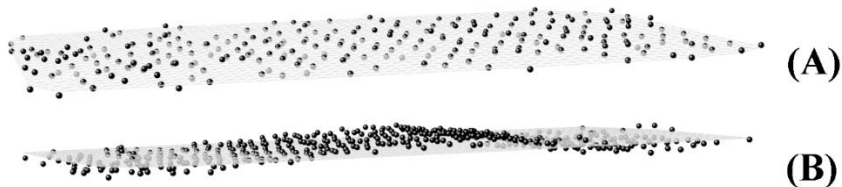


**Figure 22:** Crystallite plane calculated from the middle (C8) atoms in the HEX/Surf/water model (A) without defect and (B) with defect

The top plane in Figure 22 is calculated from atoms lying almost in one plane, while the other plane is computed for a crystallite with a defect. In both cases the resulting plane correctly represents the true plane of the crystallite.

Given a known normal vector of the crystallite plane, it is possible to calculate  $\theta$ . The tilt angle of each molecule in the crystallite is defined as the angle between the vector  $\overrightarrow{C_3C_{13}}$  (Figure 20, A) and the plane normal (Figure 23).

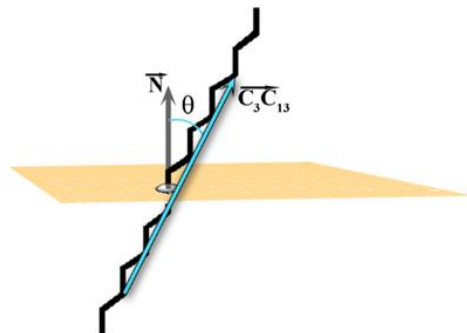


**Figure 23:** Illustration of  $\theta$ . The grey arrow is the normal vector of the plane, and the arrow in cyan is the vector  $\overrightarrow{C_3C_{13}}$  representing the long molecular axis of the alkyl chain

The vector  $\overrightarrow{C_3C_{13}}$  is chosen because it is parallel to the long axis of the molecule when all torsion angles are in *trans* conformation. The  $\theta$  (in rad) is calculated by the formula:

$$\theta = \arccos \frac{\vec{N} \cdot \overrightarrow{C_3C_{13}}}{|\vec{N}| \cdot |\overrightarrow{C_3C_{13}}|} \quad (46)$$

The procedure described so far calculates the evolution of  $\theta$  for each molecule in the crystallite for each frame of the trajectory, which can then be averaged over time (Figure 24, A). Also, the values for all molecules can be averaged across each frame of the trajectory (Figure 24, B). Thus, information about  $\theta$  over time and space is obtained. The standard deviations of the time-averaged  $\theta$  for each molecule are used to estimate the mobility of individual molecules in the crystallite. The standard deviations of the time-averaged  $\theta$  evolution indicate the degree of ordering in the crystallite as a function of time.

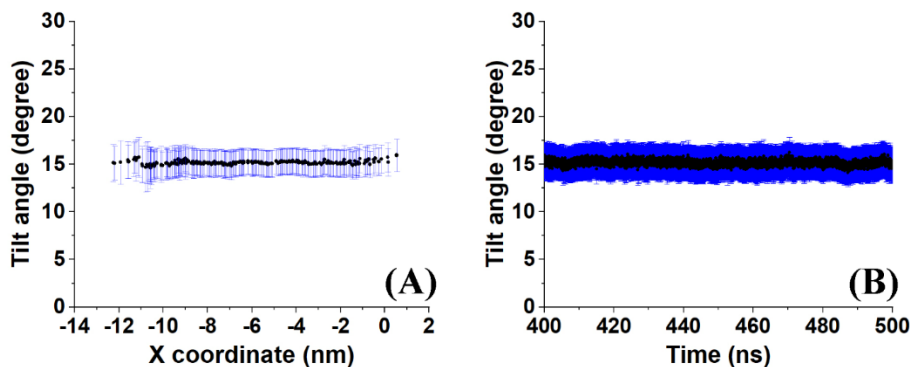


**Figure 24:** Illustration of (A) time-averaged  $\theta$  of molecules in a HEX/Surf/water crystallite and (B) the evolution of the average angle of molecules in the crystallite

Ryckaert et al.<sup>14</sup> calculate similar angles but in the procedure used in their work the values of the angles depend on the coordinate system. In this case, the tilting of the molecules will coincide with  $\theta$  only if the plane of the crystallite is orthogonal to the  $z$ -axis of the coordinate system. In the method described here, this restriction is overcome, making it more versatile.

#### 4.6. Crystallite preparation for 2D Voronoi analysis

The COMs of the molecules in the crystallite are used as key points to perform 2D Voronoi analysis.<sup>38,39</sup> For the analysis, the COMs are assumed to lie in a single plane, which is not true in the studied systems due to the thermal motion of the molecules and possible defects in the crystallite.

Therefore, to generate a set of key points (one for each molecule) that lie in the same plane, the intersection of the  $\overrightarrow{C_3C_{13}}$  vector with the crystallite plane is calculated (eq. (45)). Since in general the planes of the crystallites are not parallel to the  $xy$  plane of the coordinate system, the points will have different values of the  $z$  coordinate, complicating the analysis. Therefore, the plane and the points therein are rotated so that they lie in the  $xy$  plane. This is achieved by constructing a rotation matrix derived from the angle between an intersection point of the plane (taken as the radius-vector in this case) and the vector  $[0, 0, 1]$  (the unit vector  $\vec{z}$ ).<sup>40</sup>

The obtained points are saved in a file as a two-dimensional array, where each row is one frame and the columns have the form: (time,  $x_1, y_1, z_1, x_2, y_2, z_2, \dots$ ). 2D Voronoi analysis can be done with the data from the file.<sup>38,39</sup> An illustration of the points generated in this way is presented in Figure 25, A.

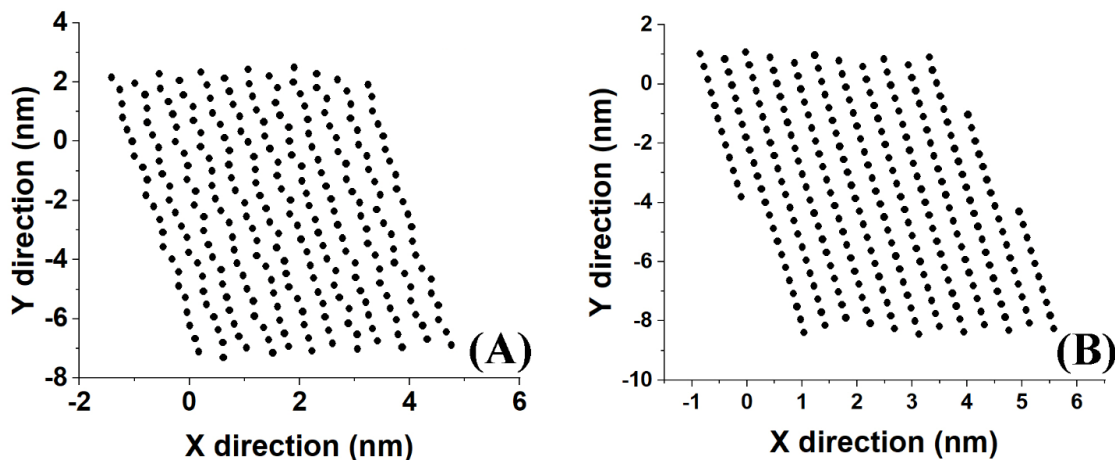


**Figure 25:** Illustration of the intersections of molecules in a crystallite with the crystallite plane (A) for one frame and (B) averaged over a 20 ns period.

As seen from the figure, the points along the rows are not aligned due to thermal motion. To overcome this artifact in the analysis, the points obtained for each frame are averaged over a

period of time (in this case 20 ns) and the newly obtained points are representative of this time period. In Figure 25, B it can be seen that after averaging, the points along the rows follow a single line, implying that the Voronoi analysis would yield more accurate data for the studied crystallite and the comparison to experimental values would be sound.

The average area of the molecules is obtained directly from the 2D Voronoi analysis, which is conducted for the real coordinates of each crystallite (without considering the periodic images). To calculate  $D$  and  $\Phi_d$ , the six nearest neighbours for each molecule obtained from the Voronoi analysis are determined (the edge molecules in the crystallite are excluded, since they do not have a full set of first neighbours). An ellipse is then constructed along each of these six points, and a value for  $D$  is calculated from the ratio of its semi-major and semi-minor axes, as described on page 7.  $\Phi_d$  is calculated as the angle drawn between the semi-major axis and the vector drawn from the centre of the ellipse and the nearest first neighbour to the semi-major axis.

#### 4.7. Calculating the relative orientation of the molecules

A key feature of rotator phases is their rotational freedom about the long axis of the molecules, which is enhanced compared to the triclinic phase.<sup>5</sup> A quantitative measure of this property for each molecule of the crystallite can be obtained from the moment of inertia tensor. The second principal axis ( $P_2$ ) indicates the mutual orientation of the molecules in the crystallite in a plane perpendicular to their long axes (Figure 26, A). This approach is used to identify rotator phases in bulk alkanes.<sup>17</sup>

The eigenvectors calculated from the tensor of the moment of inertia for each molecule form an orthogonal basis set, where the vector with the highest eigenvalue ( $P_1$ ) is parallel to the long axis of the molecule, and the vector with the second highest eigenvalue ( $P_2$ ) indicates the orientation of the bonds in space (Figure 26, C). If the long axes of the molecules are parallel to the  $z$  axis, then  $P_2$  will designate the orientations of the C-C bonds in the molecules in the  $xy$  plane.

In the method described here, the crystallite is rotated so that the molecules align parallel to the  $z$ -axis of the coordinate system as described in Sect. 4.6.  $P_2$  is then calculated for each molecule and the angles between it and the  $x$  and  $y$  axes of the coordinate system are determined. This is repeated every  $n$  frames of the trajectory, producing a movie showing the evolution of the intermolecular orientation of the molecules in the crystallite. With this method, it is also possible to identify transitions occurring during the simulation, both from liquid to solid state and between different solid-state arrangements (Figure 26, B, C).

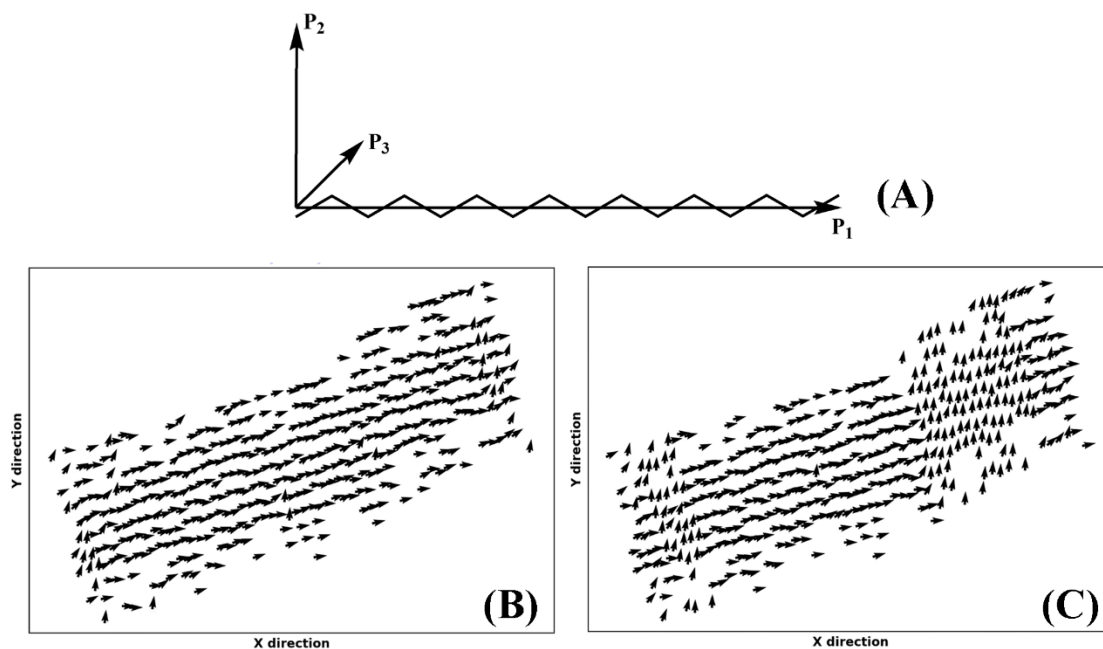


**Figure 26:** (A) Illustration of the three principal axes describing the orientation of the molecule in space; orientation of  $P_2$  in the  $xy$  plane of crystallite molecules (B) in the crystal-like state and (C) in the state of partial transition of the crystallite from one ordered state to another.

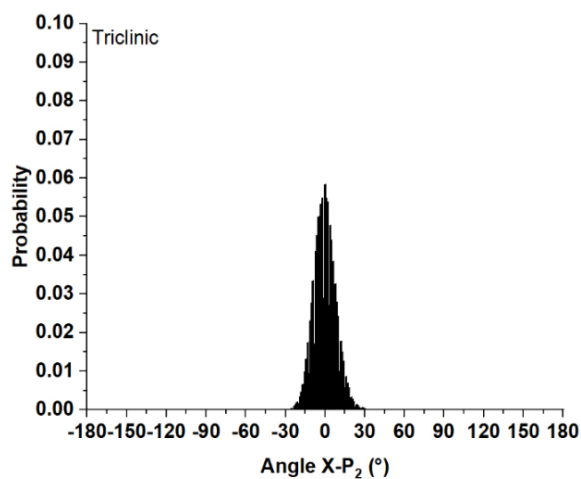


**Figure 27:** Histogram of the angles of  $P_2$  with the  $x$ -axis of the coordinate system over a period of 100 ns.

Applied in this way, the analysis is useful for assessing the stability of the phase state of the crystallite but it cannot quantify the degree of rotational freedom of the molecules within it. This can be achieved by constructing a histogram of the angles of all molecules in the crystallite with respect to the  $x$  axis of the coordinate system for the entire studied period (Figure 27). The standard deviation calculated from the Gaussian function fitted to the histogram is a quantitative measure of the degree of rotational freedom in the crystallite for the studied time period.



The developed analysis describes the type and degree of ordering of the molecules in the crystallites, the evolution of the ordering over time, and allows the determination of the phase state of the solid state entities.

#### 4.8. Validation of the used force field

Due to the non-trivial nature of the scientific problem investigated in the thesis, namely, the description of a phase transition by classical MD simulations, it is necessary to select a force field that can reproduce such a process. The four force fields tested are CHARMM36,<sup>15</sup> Lipid17,<sup>41</sup> AMBER99<sup>42</sup> and OPLS-AA.<sup>16</sup> For systems where water is also present, TIP4P is always employed,<sup>19</sup> which is compatible with all four force fields. The selected force field needs to fulfil the following three criteria: (i) after heating the system to 350 K, a phase transition from a regular lattice to an isotropic liquid should be observed; (ii) once the systems are in the isotropic liquid state, their bulk mass density should reproduce the experimental value or be close to it; (iii) a freezing process has to take place in the systems after cooling them to different temperatures between 273 K and 300 K.

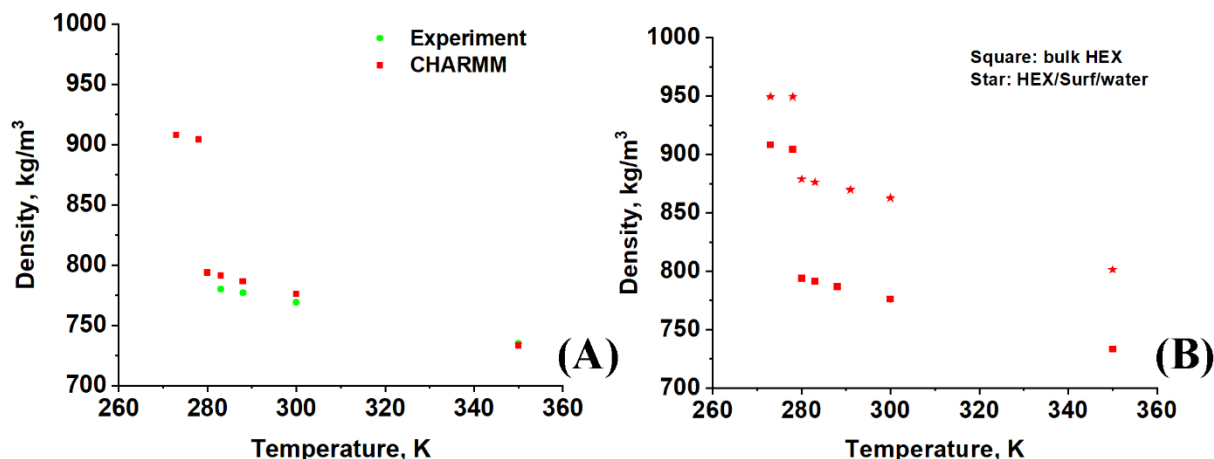


**Figure 28:** Bulk mass density of model systems at different temperatures averaged over the 480-500 ns period of the corresponding MD trajectory with CHARMM36 force field: (A) bulk HEX and (B) HEX/Surf/water; experimental values are taken from Outcalt *et al.*<sup>43</sup>

Of the four studied force fields, CHARMM36 is the only one where all the expected phase transitions are observed, namely from a regular lattice to an isotropic liquid and then from an isotropic liquid to an ordered state at low temperature. The liquid  $\rightarrow$  solid transition is characterised by the abrupt change in density at temperatures of 278 K or lower for both types of model systems (Figure 28). Also, CHARMM36 is able to reproduce the experimental density of liquid hexadecane almost quantitatively, as shown in Figure 28. The other three force fields fail to feature at least one of the two phase transitions (Figure 29).

From the data presented so far, it is seen that only CHARMM36 succeeds in describing the systems both qualitatively and quantitatively. Due to the good agreement of the density with the experimental data, this classical potential can be used to evaluate the thermodynamic characteristics of alkane-containing systems.

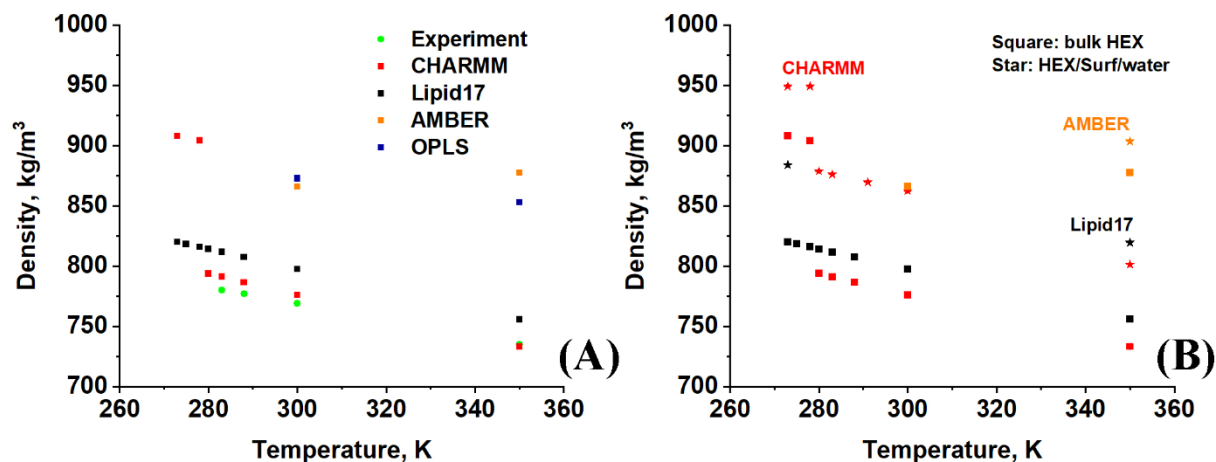


**Figure 29:** Bulk mass density of model systems at different temperatures averaged over the 480-500 ns period of the corresponding MD trajectory: (A) bulk HEX for all force fields studied and (B) HEX/Surf/water and bulk HEX only with the force fields used for both model types.

The good performance of CHARMM36 can be explained by a number of reasons: (i) the force field parametrization aims at an accurate representation of the supramolecular organization of lipid bilayers in multiple phase states; (ii) the parametrization in CHARMM36 is based on an accurate balance of the intermolecular interaction energies between the lipids themselves and between the lipids and the solvent; (iii) the torsional potential of the lipid tails in CHARMM36 is parameterized over a large set of conformations and the energy for the *trans/gauche* transition is fitted to quantum mechanical calculations; (iv) the weight of electrostatic interactions is relatively underestimated compared to the other three fields, since CHARMM36 uses partial atomic charges derived from a semiempirical method rather than the time-consuming (and more accurate) RESP procedure. The reasons presented and the data described in the chapter show that CHARMM36 is the best choice for the force field, and it has been used for all the systems presented in the thesis.

The two types of model systems are cooled from 300 K to various lower temperatures, with the highest temperature at which a liquid  $\rightarrow$  solid transition is always observed being 278 K. All production trajectories that are structurally analysed are obtained at 278 K.

#### 4.9. Analysis of the physical chemical properties – temperature, enthalpy and density

One of the main objectives of the research in the thesis is the correct modelling of the phase transition from liquid to solid state. The transition is expected to be of first order and is characterized by an abrupt change in enthalpy and density of the system (Figure 30, B, C).<sup>2,11</sup>

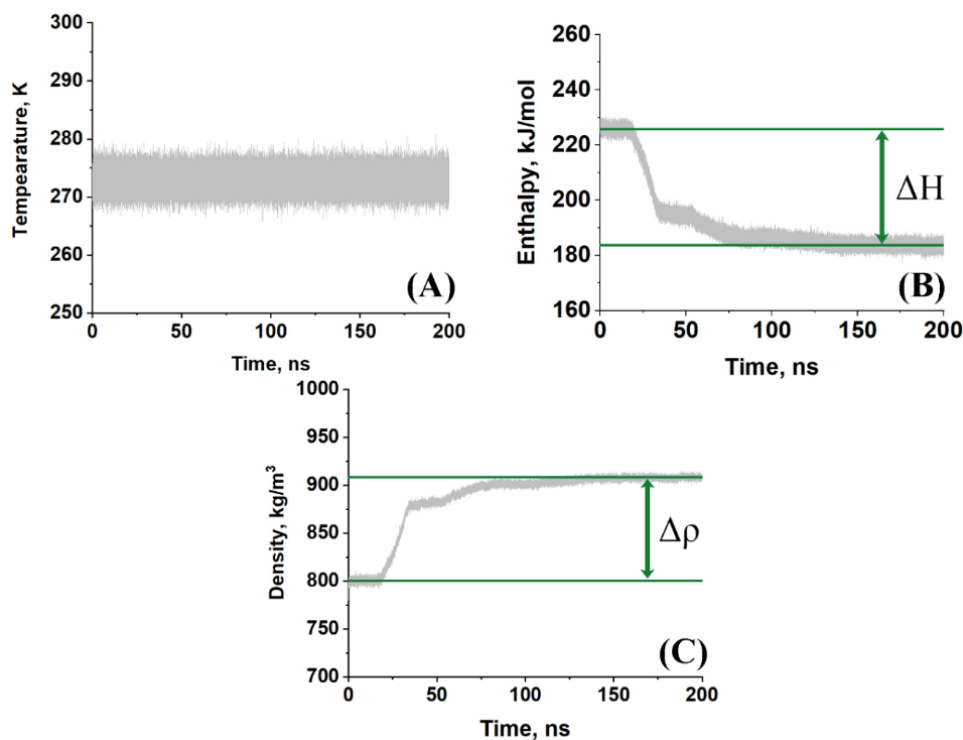


**Figure 30:** Illustrative evolution of monitored physical chemical parameters during crystallisation of bulk HEX upon cooling from 300 K to 278 K: (A) temperature (B) enthalpy (C) bulk density.

At the same time, the temperature should not deviate from its mean value (Figure 30, A). This behaviour is observed in all model systems, in both bulk HEX and HEX/Surf/water.

**Table 12:** Enthalpies of the phase transitions ( $\Delta H$ , J/g) observed in the MD simulations;  $T_i$  is the temperature from which the system is cooled and  $T_f$  is the temperature at which the productive part of the simulation is conducted; experimental data are taken from Cholakova et al.<sup>5</sup>

System	$T_i \rightarrow T_f$ , K	$\Delta H$ , J/g	$\frac{\Delta H}{\Delta H_{\text{exp}}}$ , %
Experiment (liquid $\rightarrow$ triclinic)		236	100
Bulk HEX	300 $\rightarrow$ 273K	188	80
	300 $\rightarrow$ 275K	170	72
	300 $\rightarrow$ 278K	193	82
	350 $\rightarrow$ 273K	168	71
HEX/Surf/water	300 $\rightarrow$ 278K	179	76
	350 $\rightarrow$ 273K	182	77

Cholakova et al. show that 65-80% of the transition enthalpy in alkane systems with an intermediate rotator phase is due to the formation of the rotator phase.<sup>5</sup> For comparison, the transition enthalpies in the simulated systems are calculated as a difference denoted with green arrow in Figure 30, C. The values (Table 12) are compared with the experimental transition enthalpy for bulk hexadecane from an isotropic liquid to a triclinic crystal.<sup>5</sup>

The calculated transition enthalpies in the simulated systems range from 71% to 82% of the experimentally determined value. This indicates that the models are in the rotator phase or are in transition from rotator to crystalline phase.

The density profiles for all systems also correspond to a transition to solid state when the temperature is 278 K or lower. After freezing, the density increases by  $\sim 100 \text{ kg/m}^3$ . This jump is similar for both types of model systems since the reorganization process is the same in both cases.

The presence of surfactant in the system does not affect the freezing point, which is in agreement with the experimental data. However, there is a deviation from the experimentally determined value by  $\sim 13 \text{ K}$ .<sup>5</sup> The latter can be attributed to two factors. The first one is the supercooling effect due to the nanoscopic size of the systems. The second reason may be due to the tendency of the force field to underestimate the phase transition temperature. Such an effect has been observed for lipid-containing systems simulated with CHARMM36.<sup>15</sup> In order to determine which of the two factors leads to the lowered freezing temperature in the calculations, an additional simulation is performed where a HEX/Surf/water system is cooled to 278 K to produce a crystal nucleus, then heated to 289 K. The system at 289 K is simulated for 500 ns with the same computational protocol as the other models. The presence of a nucleus in the system results in solid crystallites throughout the hexadecane phase of the system (Figure 32), indicating that the reason for the lower freezing temperature is the nanoscopic nature of the model systems.

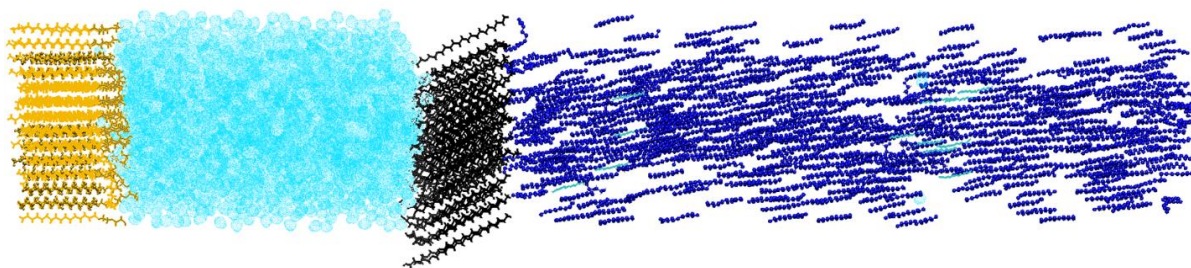


**Figure 32:** *HEX/Surf/water after 500 ns MD simulation at 289 K with initial crystal nucleus; hexadecane is represented by beads, surfactant tails by bold lines, surfactant heads by thin lines and water by bubbles.*

#### 4.10. Nucleation analysis

As an initial step in the structural analysis, the time at which the freezing of the system begins is determined, namely the formation of the crystal nucleus. This is achieved by measuring the distances between carbon atoms 3 and 14 (Figure 20, A) for each molecule in each frame of the bulk HEX and HEX/Surf/water trajectories.

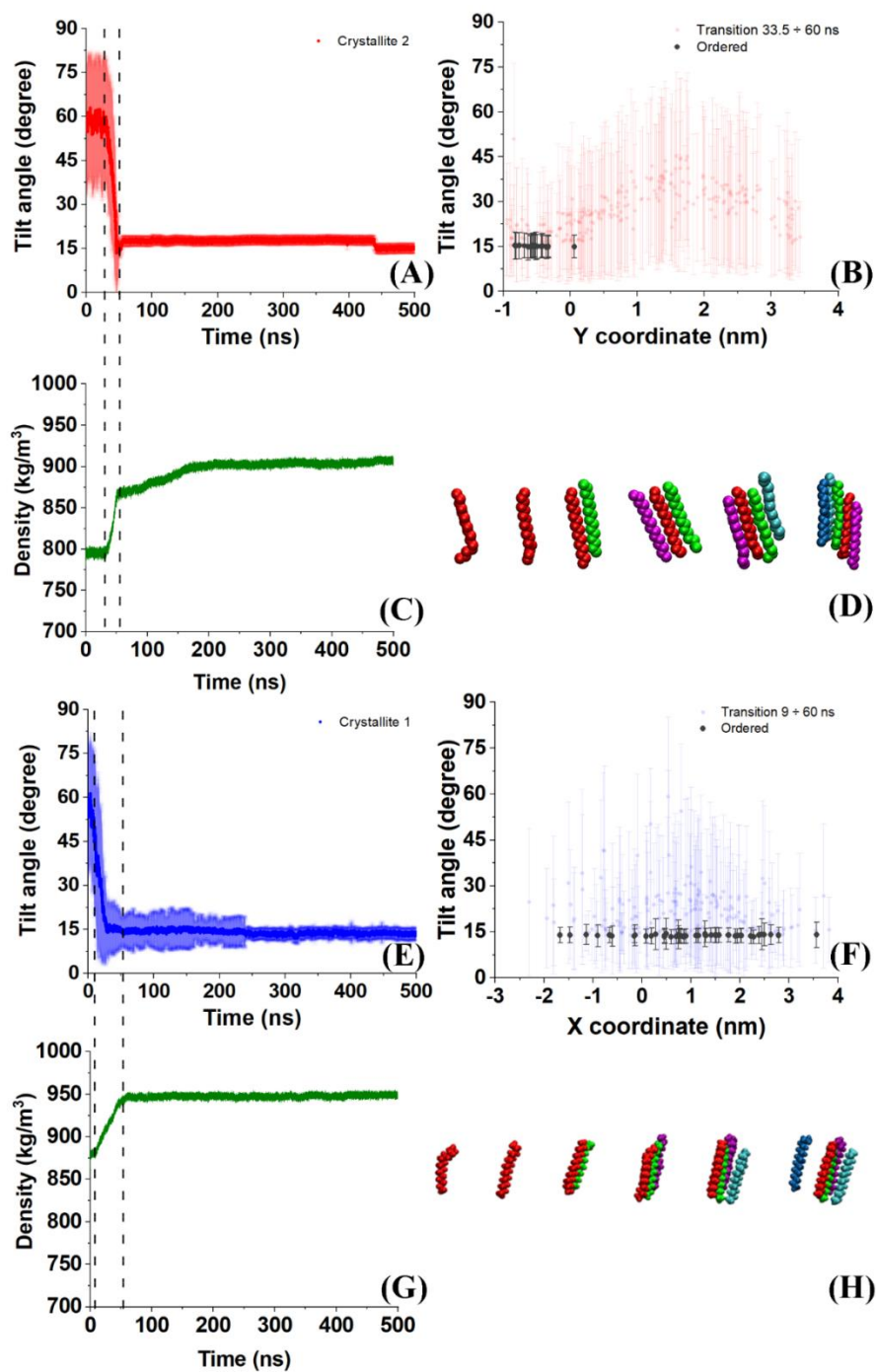


**Figure 33:** Analyses to determine the onset of the freezing process and the position of the crystal nucleus in (A to D) bulk HEX and (E to H) HEX/Surf/water: (A, E) evolution of  $\theta$  of the molecules composing the first crystallite in the system; (B, F) time-averaged  $\theta$  for individual molecules in the first crystallite around the freezing time of the system (33-60 ns for bulk HEX and 9-60 ns for HEX/Surf/water); (C, G) evolution of bulk density; (D, H) illustration of the first 5 molecules of the crystal nucleus.

When this distance reaches a steady magnitude of 1.4 nm, the molecule is assumed to be frozen. This value would only be reached if all C-C-C-C torsion angles are in *trans* conformation, which is consistent with literature evidence that alkanes stretch upon freezing.<sup>44</sup> The onset of the freezing process is also confirmed by the evolution of  $\theta$  (Chapter 4.5), which is correlated with the density profile of the corresponding system (Figure 33, A, C, E, G). The position of the nucleus in space is determined from the time-averaged tilt angles of the molecules in a given system (Figure 33, B, F).

Analysis of the data obtained shows that in bulk HEX the three monitored parameters are highly correlated, whereas in HEX/Surf/water the density probably reflects the change in the structure of all components in the system, not just the crystallite formed.

Comparing the average tilt angles of the molecules in the first crystallites of the two systems, two types of nucleation are observed (Figures 33B, 33F). In bulk HEX, the nucleating molecules are in close proximity in space (Figure 33C), which is an example of homogeneous nucleation.<sup>9</sup> Conversely, in HEX/Surf/water the molecules that are frozen first during the transition are scattered along the entire length of the crystallite. This is due to the surfactant surface being frozen at 300 K and serving as a template. This is in perfect agreement with the known foundations of crystallization for these two types of systems.<sup>9</sup> This analysis also greatly expands the knowledge at the molecular level of the nucleation mechanisms of n-alkanes, which are only briefly addressed in the work of Esselink et al.<sup>45</sup>

The results from the nucleation analysis show that the developed criteria are accurate enough to separate the molecules in the nucleus at the time of formation, regardless of the type of model system. The procedure also allows determining the position of the nucleus in space.

## 4.11. Structural analysis of the solid phases

### 4.11.1. Overall structuring in the frozen systems

Visual inspection of the trajectories after the end of the phase transition reveals a polycrystalline structure in both model systems. This is illustrated in Figure 34, where each crystallite is indicated by colour. A small fraction of molecules in both bulk HEX (< 3%) and HEX/Surf/water (< 7.5%) remains disordered and trapped between the ordered layers for the duration of the simulations. This observation indicates that the process of intermolecular organization is still ongoing. The latter is also true for individual crystallites. They vary in size and even visually some are more ordered than others. Crystallite 2 in bulk HEX and crystallite 1 in HEX/Surf/water are the largest in the respective model system. The former contains 60% of all molecules and the latter 36% of the organic fraction. It should be noted that these two crystallites are formed from the initial crystal nucleus.

In order to characterise the crystallites in the systems, they need to be isolated and analysed separately, the procedure for which is described in Chapter 4.3.

In order to analyse the global structure of each crystallite, the radial distribution functions (RDFs) between the centres of mass of the HEX molecules/surfactant alkyl chains are calculated. The profiles of these functions are then compared with those of reference crystals in the triclinic phase and in the orthorhombic rotator phase of bulk hexadecane.

The data for the reference crystals are obtained from separate MD simulations of the two regular structures that are known for hexadecane. One is an ideal triclinic crystal (Figure 35A), which is the thermodynamically most stable phase of solid hexadecane.<sup>5</sup> The second (Figure 35B) is a rotator phase  $R_1$ , found experimentally for HEX at a surfactant-stabilised interface with water.<sup>5</sup> It is characterized by a face-centred orthorhombic lattice with crystallographically determined parameters. These two regular crystallites are used as references for comparison to allow the determination of the type of solid-state structure occurring in the bulk HEX and HEX/Surf/water crystallites after freezing.

It should be noted that the reference rotator phase undergoes structural changes after 500 ns (molecules tilt relative to the plane of the layers), which corresponds to the initial stages of the phase transition from rotator to triclinic phase. This is accompanied by a herringbone-type stacking of pairs of adjacent layers at an angle to each other. The transition is already initiated in the early stages of the simulations in the rotator phase ( $R_1 \rightarrow T$ ) and in the orthorhombic crystal ( $O \rightarrow T$ ). Transitions to and from rotator phases are also observed in previous studies,<sup>11,46,47</sup> but not this particular one. The triclinic crystal remains unchanged for the entire simulation period (Figure 35, A).

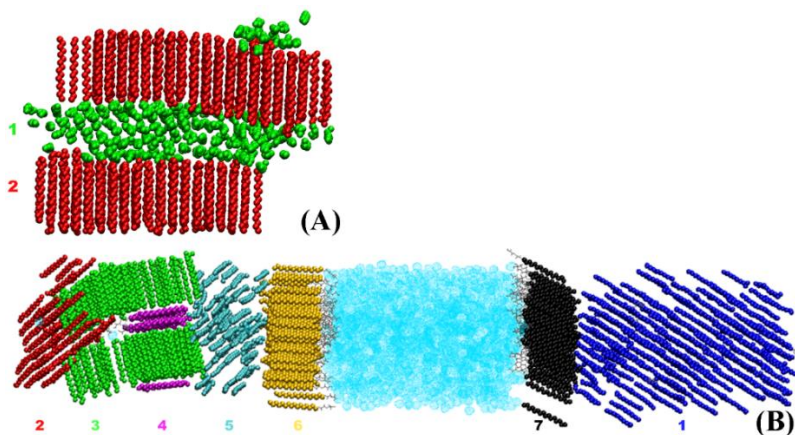


**Figure 34:** Illustration of crystallites in the model systems (A) bulk HEX and (B) HEX/Surf/water. Each colour represents an individual crystallite formed after cooling from 300 K to 278 K and a subsequent simulation of 500 ns at 278 K in an NPT ensemble.

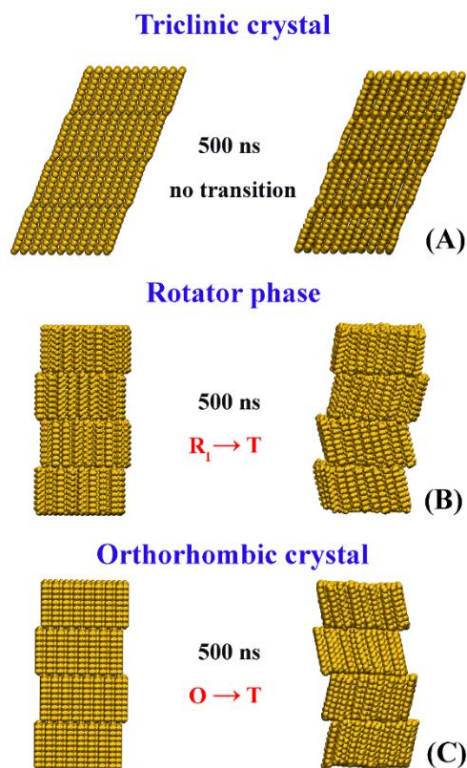


**Figure 35:** Illustration of the three reference structures of bulk HEX: (A) triclinic crystal built from crystallographic data after 500 ns MD simulation; (B) rotator phase (orthorhombic lattice) constructed from crystallographic data after 500 ns MD simulation; (C) initial orthorhombic crystal (orthorhombic lattice without random rotation of molecules about their long axes) after 500 ns MD simulation.

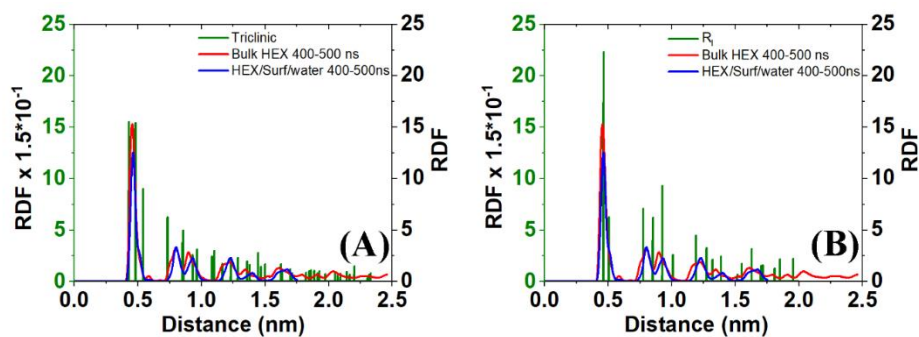


**Figure 36:** 3D radial distribution functions between the centres of mass of the aliphatic chains in the largest bulk HEX (red) and HEX/Surf/water (blue) crystallites. They are compared with reference systems from (A) bulk HEX in the triclinic phase from crystallographic data;<sup>48</sup> (B) bulk HEX in the orthorhombic rotator phase from crystallographic data.



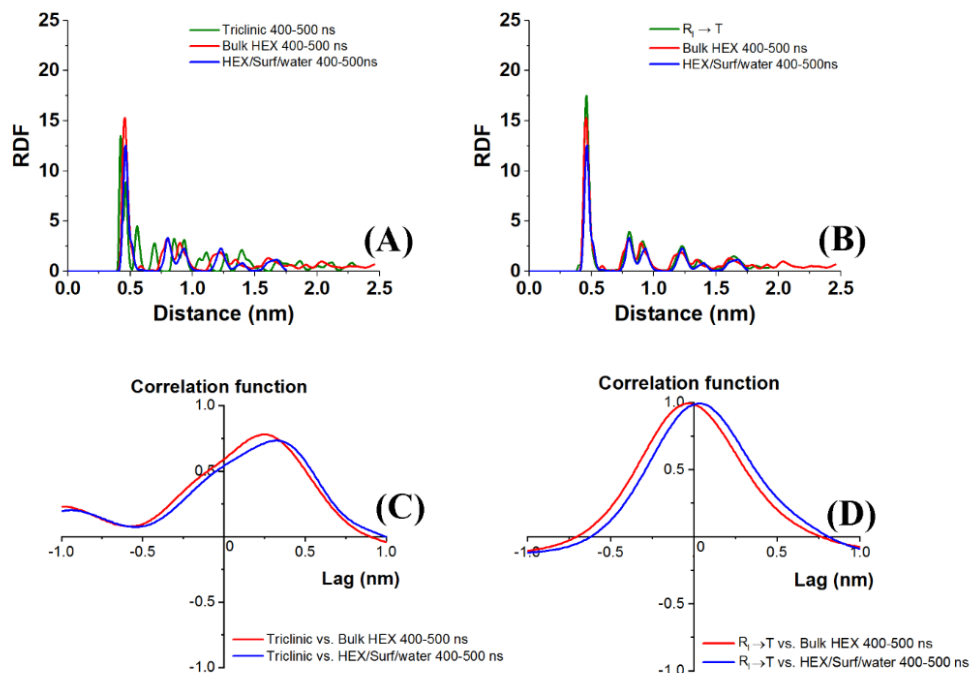


**Figure 37:** 3D radial distribution functions between the centres of mass of the aliphatic chains in the largest bulk HEX (red) and HEX/Surf/water (blue) crystallites. They are compared with reference systems from (A) bulk HEX in the triclinic phase after 500 ns MD simulation; (B) bulk HEX in the orthorhombic rotator phase after 500 ns MD simulation. In all plots, reference systems are in green; all RDFs are normalized to the number of molecules and box volume to allow for comparison. Correlation functions of the RDF profiles of the two crystallites with those of the (C) triclinic or (D)  $R_1 \rightarrow T$  reference system.

Comparison of the bulk HEX and HEX/Surf/water crystallites with the reference crystallites shows that the MD-generated crystallites are in the  $R_1 \rightarrow T$  transition. Even correlation to the initial crystallographic structures (Figure 36A and 36B) reveals that the RDF profiles of the two crystallites are much better represented by the orthorhombic phase peaks than by those of the triclinic crystal. This statement is confirmed by the averaged data from the reference trajectories. The RDFs of the crystallites clearly overlap with the  $R_1 \rightarrow T$  model (Figure 37, C). In the case of the triclinic crystal, the number and position of peaks do not match those observed in the crystallites.

To quantify the correlation between the respective RDF profiles, cross-correlation functions (CCFs) are calculated with the TISEAN software package<sup>49</sup> (Figure 37, C, D)). The CCFs reveal almost perfect correlation at small lags with the  $R_1 \rightarrow T$  transition in the two most ordered crystallites. In contrast, the CCF of the triclinic crystal after 500 ns of simulation with bulk HEX and with HEX/Surf/water is smaller in peak value (about 0.8) and the peak is significantly shifted toward larger delays. This confirms the qualitative conclusion drawn above.

The profiles of  $R_I \rightarrow T$  and  $O \rightarrow T$  are relatively close, but the crystallites studied are more similar to  $R_I \rightarrow T$  (Figure 38).

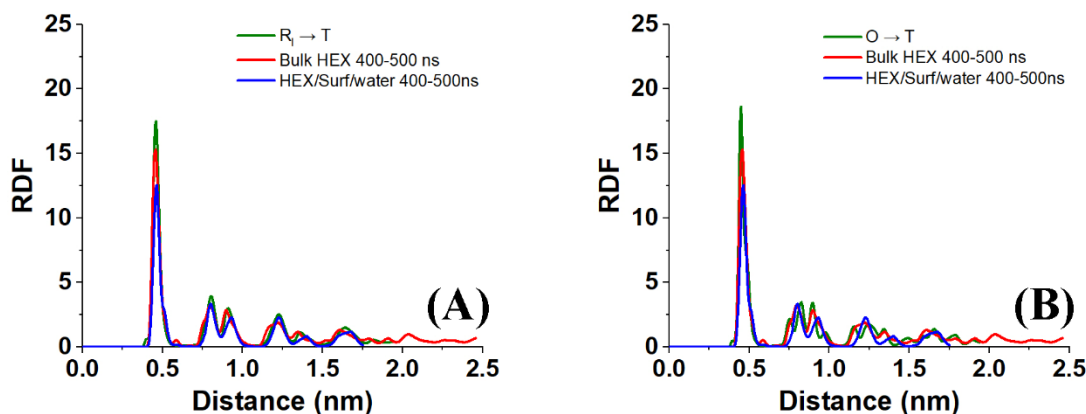


**Figure 38:** Comparison between the 3D RDF of the two largest crystallites in bulk HEX and HEX/Surf/water and (A) an orthorhombic rotator phase simulated with MD for 500 ns; (B) an orthorhombic crystal (molecules are not randomly rotated along their long axis in the initial configuration) simulated with MD for 500 ns.

It should also be noted that the rotator-to-crystal phase transition occurs for both bulk HEX and HEX/Surf/water. The RDF peaks of the two model systems are practically identical and match those of the reference rotator phase after 500 ns MD simulation ( $R_I \rightarrow T$  transition). This is an important observation that indicates at the molecular level the formation of rotator phases upon freezing of hexadecane-containing systems.

#### 4.11.2. Local arrangement of the alkyl chains in the crystallites

An important structural parameter to determine whether a crystallite is in a rotator phase is the tilt angle of the molecules relative to the plane of the crystallite (Chapter 4.5). Figure 42 shows the evolution of the mean  $\theta$  and the time-averaged  $\theta$  of each molecule in the respective crystallites. Again, crystallite 2 of bulk HEX and crystallite 1 of HEX/Surf/water are characterized by the most stable average tilt (Figure 42, A, C). The former shows an increase of  $\sim 2^\circ$  at  $\sim 430$  ns. This shift is accompanied by further ordering in the crystallite, as evidenced by the smaller standard deviation.

The average tilt angles of the individual molecules in each crystallite (Figure 42, right panel) are similar, confirming further the homogeneous intermolecular arrangement. The degree of ordering of the crystallites is very sensitively reflected in the standard deviations. The standard deviation is about 1.5 times larger ( $4.7^\circ$ ) in crystallite 1 of bulk HEX than in crystallite 2 (about  $3.4^\circ$ ). Therefore, this parameter can be used as a quantitative measure of the degree of ordering in the studied systems. In HEX/Surf/water this hierarchy is as follows: crystallite 1 ( $1.6^\circ$ ) > crystallite 3 ( $1.7^\circ$ ) > crystallite 7 ( $1.9^\circ$ ) > crystallite 6 ( $2.4^\circ$ ) > crystallite 2 ( $3.0^\circ$ ) > crystallite 4 ( $18.2^\circ$ ). The smaller standard deviations in the HEX/Surf/water model suggest that smaller changes in the

structure occur, related to the slower crystallization process due to the stabilization of the rotator phase by the surfactant surfaces.<sup>5</sup>

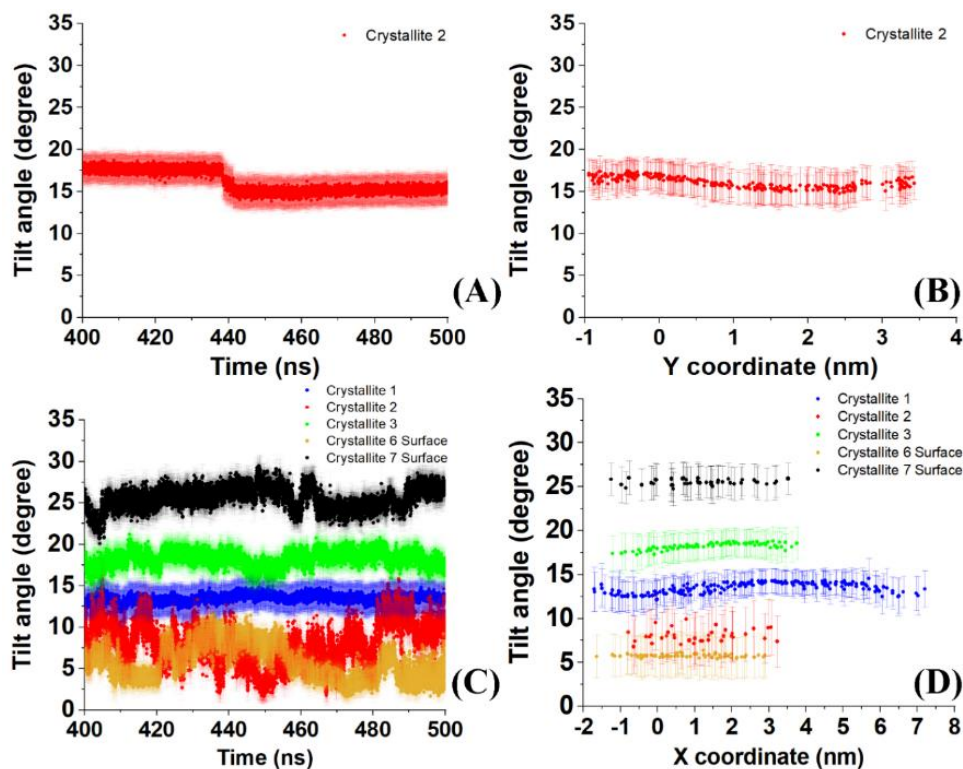


**Figure 42:** Evolution of the tilt angle, averaged over all molecules, with respect to the plane of each crystallite as a function of time in (A) bulk HEX and (C) HEX/Surf/water. Time-averaged tilt angle of each molecule as a function of its x- or y-coordinate in (B) bulk HEX and (D) HEX/Surf/water. Only data for well-structured crystallites of (top) bulk hexadecane and (bottom) hexadecane-surfactant system are shown.

#### 4.11.3. Voronoi analysis

Another important characteristic of the phase state of crystallites is the average distance to the first neighbours. This parameter can be calculated after performing a 2D Voronoi analysis as described in Chapter 4.6.

Figure 45 shows the average distance to the first neighbours in crystallite 2 of bulk HEX and in crystallite 1 of HEX/Surf/water. These are superimposed on the profiles for the corresponding average distances in the initial reference triclinic crystal and in the rotator phase, as well as on those averaged over the last 100 ns of the reference MD trajectories. The peaks corresponding to the rotator phase after 500 ns of the MD simulation best describe the positions of the first neighbours in the two crystallites (Figure 45, D), whereas comparison with the triclinic phase (Figure 45, C) reveals almost no matches, confirming the results obtained from the RDF.

Furthermore, the nearest-neighbour distance profiles clearly show a deformation that is between that characteristic of the  $R_1$  rotator phase (figure 45B, green line) and the triclinic crystal (figure 45, green line).

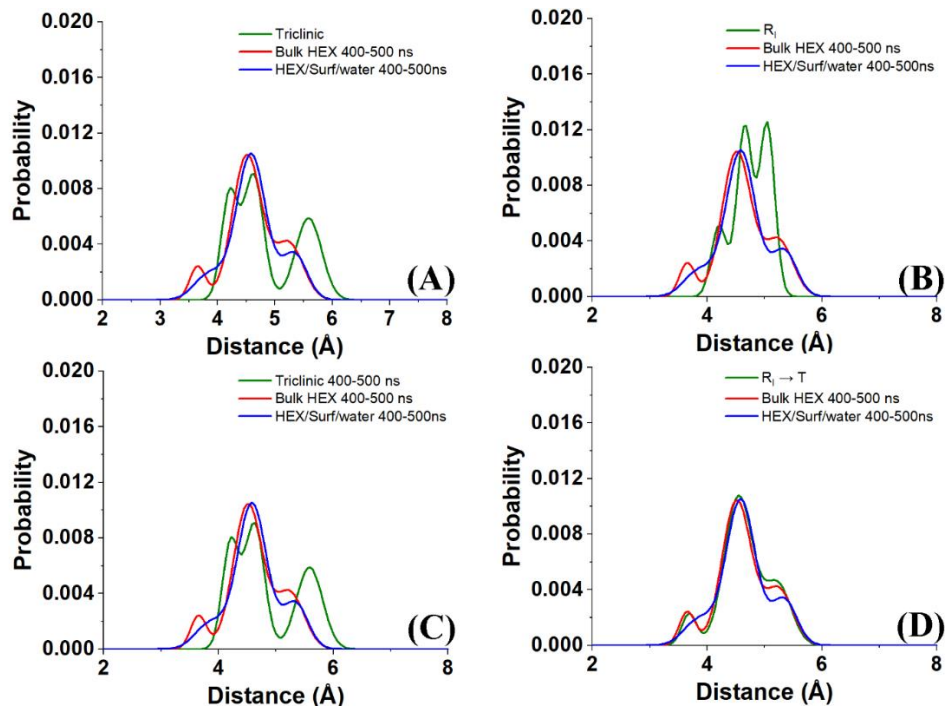


**Figure 45:** Time- and molecule-averaged distributions of distances to first neighbours for the largest crystallite of each of the two model systems compared with (A) triclinic crystal of bulk HEX; (B) orthorhombic rotator phase of bulk HEX; (C) reference triclinic crystal of bulk HEX after 500 ns MD simulation; (D) reference orthorhombic rotator phase of bulk HEX after 500 ns MD simulation.

#### 4.11.4. Rotational order in the crystallites

The rotational freedom can be represented by the second principal axis of the molecules for each crystallite. The procedure for calculating this parameter is described in Chapter 4.7.

Figure 48 shows representative snapshots illustrating the intermolecular orientation in bulk HEX upon cooling to 278 K and further simulation at this temperature and of the reference triclinic crystal at the beginning of the production simulation at 278 K and after 500 ns. A transition from an isotropic liquid to an ordered (crystal-like) structure is observed in the crystallite from the model system. This is reflected in the mutual orientation of the molecules, which at the beginning of the simulation rotate freely about their long axis (Figure 48, A). After freezing, the rotations of the molecules continue to be relatively intense for ~30 ns, suggesting a short-lived rotator phase. After that, the molecules remain oriented in one direction with some random rotations due to thermal fluctuations (Figure 48, B). Such thermal fluctuations are also observed in the triclinic crystal.

However, the magnitude of the rotations is much smaller and the frequency of rotations of larger magnitude is practically negligible. This confirms the above conclusions that the molecules in bulk HEX crystallite 2 are in the stage of active transition to the crystalline phase.

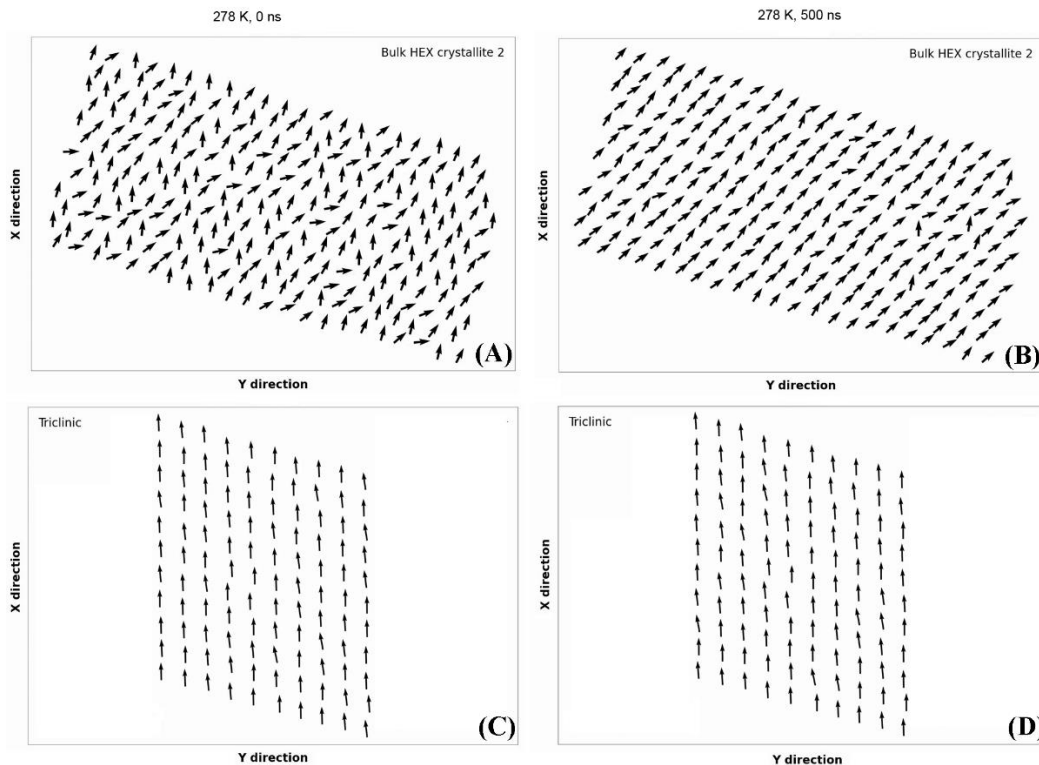


**Figure 48:** Representative  $P_2$  orientation of each alkane molecule in (top) bulk HEX crystallite 2 and (bottom) the reference triclinic crystal: (A) initial liquid state of bulk HEX, (B) final ordered state of bulk HEX, (C) initial and (D) final structure of the reference crystal.

On the other hand, crystallite 1 of HEX/Surf/water first transitions from the liquid state to the rotator phase (Figure 49, B). The same orientation of the molecules with respect to each other as in the reference rotator phase is observed (Figure 49, F). Later in the trajectory (at about 200 ns), a second transition from the rotator phase is observed that is similar to the ones in bulk HEX crystallite 2 and in the triclinic crystal (Figure 49, C).

After the second transition, equilibrium is established between the two ordered states. However, the crystalline state is more pronounced (Figure 49, D). The first phase formed after freezing closely resembles the crystal structuring of the reference rotator phase. This HEX/Surf/water behaviour is consistent with the longer lasting rotator phase recorded in the experiments than in bulk HEX, followed by rearrangement to a more ordered state. The new insight from the  $P_2$  orientation analysis is that the second transition is a collective process that must be undertaken by many molecules simultaneously.

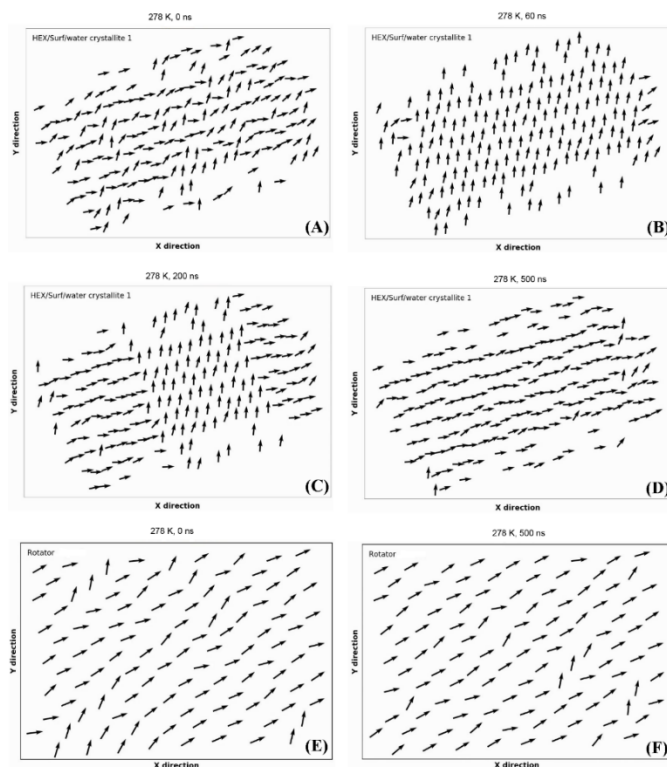


**Figure 49:** Representative  $P_2$  orientation of each alkane molecule in (top and middle) HEX/Surf/water crystallite 1 and (bottom) the reference rotator phase: (A) initial liquid state of HEX/Surf/water, (B) first rotator phase formed in HEX/Surf/water, (C) coexistence of two ordered phases in HEX/Surf/water; (D) second more ordered phase formed in HEX/Surf/water, (E) initial and (F) final structure of the reference rotator phase.

## 4.12. Determining the type of solid phases obtained at different cooling rates

### 4.12.1. Analysed systems

This subchapter describes the results of an in-depth structural analysis of the two model systems presented in the previous chapter. Model systems with the same molecular composition that are cooled from 300 K to 278 K at different rates, namely 0.1 K/ps, 0.01 K/ps and 0.001 K/ps, and then simulated in an NPT ensemble for 1  $\mu$ s are also analysed. In this way, the effect of the cooling rate on the formation and type of the resulting ordered phase can be investigated. For each system, one representative crystallite is selected which is the most ordered of the large crystallites obtained in the given system.

The eight investigated structures allow a statistically significant conclusion to be drawn about the intermolecular organization upon cooling of hexadecane-containing systems. The two largest crystallites studied for bulk HEX and HEX/Surf/water are presented in Figure 50.

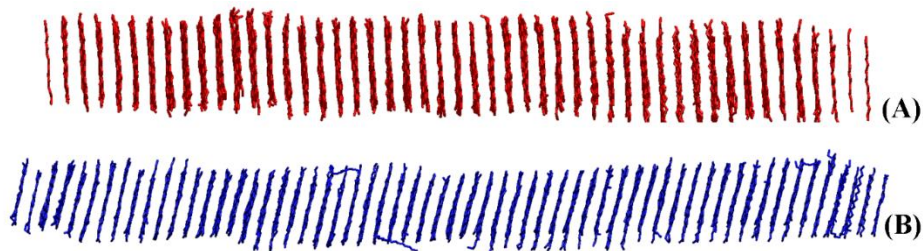


**Figure 50:** Illustration of two of the studied crystallites after reconstructing the actual coordinates of the molecules with the procedure described in Chapter 4.4; (A) Bulk HEX at 0.001 K/ps and (B) HEX/Surf/water at 0.001 K/ps.

#### 4.12.2. Enthalpy and mass density analysis of the model systems

In all studied systems, a sharp decrease in enthalpy along with an abrupt increase in mass density is observed, indicating a first-order phase transition. The drop in enthalpy is calculated for each system and compared with the experimental value for the transition from isotropic liquid to triclinic crystal for hexadecane, as described in Chapter 4.9. The data are presented in Table 14.

Most systems fall within the rotator phase range with three exceptions, which are bulk HEX at 0.001 K/ps, HEX/Surf/water at 0.01 K/ps, and HEX/Surf/water at 0.001 K/ps. These three systems have a decrease in enthalpy that is more than 80% of the experimental value. This is an indication that these three crystallites are at a more advanced stage of the transition to the triclinic crystal phase relative to the others. This assumption will be further confirmed by structural analyses.

To evaluate the effect of cooling rate on the freezing of the systems, the ratio between the number of molecules in the largest crystallite and the total number of molecules in the system at each cooling rate is calculated. The data are presented in Figure 52.

**Table 14:** Decrease in enthalpy ( $\Delta H$ ) in the model systems after transition from liquid to solid state; experimental data are given for comparison.<sup>5</sup>

System	Cooling rate, K/ps	$\Delta H$ , J/g	$\frac{\Delta H}{\Delta H_{exp}}$ , %
Experiment (liquid $\rightarrow$ triclinic crystal)		235.7	100.0
Bulk HEX	1	176.5	74.9
	0.1	164.6	69.8
	0.01	173.0	73.4
	0.001	197.0	83.6
HEX/Surf/water	1	184.3	78.2
	0.1	182.6	77.5
	0.01	189.2	80.3
	0.001	201.9	85.7

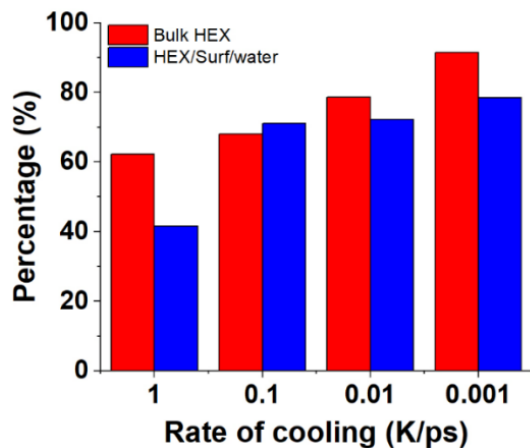


**Figure 52:** Percentage of molecules in the largest crystallite at each cooling rate. Percentages for HEX/Surf/water systems are calculated from the number of hexadecane molecules only for direct comparison with bulk HEX.

The data show a clear trend - slower cooling rates lead to the formation of larger crystallites, although from an experimental point of view all cooling rates are extremely fast. This is consistent with expectations from first principles of crystallisation theory.

#### 4.12.3. Ratio of *gauche/trans* conformations in the crystallites

As molecules transition from a liquid to a crystalline structure, their freedom of movement is limited and the energy required for a conformational change increases. Thus, the decrease in *gauche* conformations indicates higher degree of order.<sup>13</sup> To distinguish more accurately the degree of ordering of the molecules in the representative crystallites, three types of torsion angles are studied: those containing a terminal methyl group (these groups have the most significant freedom of movement), those containing a terminal methylene group (the second (C2) and fifteenth (C15) carbon atom in a hexadecane), and those containing internal methylene groups. The percentages of *gauche* conformations in each crystallite in the two references and in all model systems for the three torsion angle categories, averaged over the last 100 ns of the simulation, are presented in Figure 53.

The values are summarized on a histogram constructed by counting the torsion angles in the three parts of each molecule separately (Figure 53, top, left). The total area of each histogram is normalized to 1. Thus, by measuring the area of the histograms in the range  $-135^\circ$  to  $135^\circ$ , the fraction of *gauche* conformations for the corresponding fragment of the molecule is obtained.

Analysis of the three groups of torsion angles shows that the most sensitive indicator of the type of ordering in the systems is the percentage of *gauche* conformations in the methyl groups. Most of the models show a significantly higher degree of mobility in the methyl groups compared to the reference triclinic phase and have values relatively close to the rotator phase. It is worth noting that in Chapter 4.1 the reference system with rotator phase is determined to be in a state of transition to the triclinic phase towards the end of the simulation. Bulk HEX at 0.1 K/ps exhibits



the highest degree of disorder among the systems in this analysis. However, this may be due to a period of active transition to the crystalline phase, which is confirmed by the other analyses (shown below). On the other hand, HEX/Surf/water at 0.01 K/ps has the lowest percentage of *gauche* conformations among all models. This indicates that the system is at an advanced stage of transition to a triclinic crystal phase, although it is not yet fully ordered.

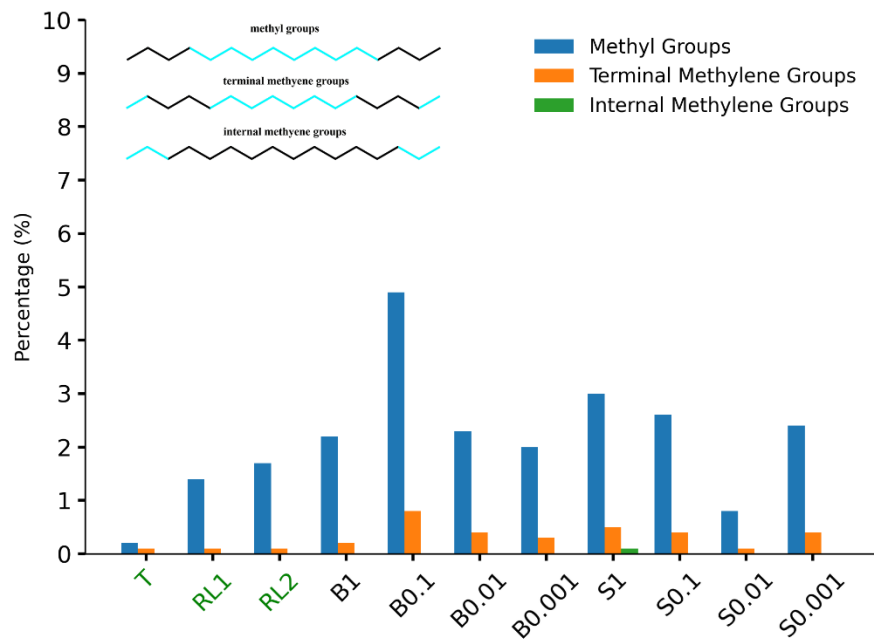


**Figure 53:** Percentage of *gauche* conformations in the studied crystallites and the two reference systems. The three types of torsion angles (in black) calculated for each molecule in the crystallites are indicated in the upper left corner.

It may be concluded from the shown results that the percentage of *gauche* conformations in the crystallites is a sensitive indicator of the degree of ordering.

#### 4.12.4. Analysis of the radial distribution functions of the crystallites

The RDFs of the model and reference systems are computed in the same way as in Chapter 4.11. In order to quantify how well each crystallite matches one of the reference systems, the Jaccard index is calculated.<sup>50</sup> It can range from 0 to 1, where 0 means that the two RDF profiles do not overlap and 1 means that they are identical. Before calculating the index, the RDFs are truncated at 1.5 nm, as the tails are very noisy and cannot be interpreted reliably. The calculated Jaccard indices are presented in Table 15.

Similar to the previous analysis, most of the crystallites show strong similarity to the reference rotator phase. The systems that are in active transition to the triclinic phase (bulk HEX at 0.1 K/ps; HEX/Surf/water at 0.01 K/ps and 0.001 K/ps) have a dramatically lower Jaccard index

with the rotator phase compared to the other crystallites. Comparison of the transition structures with the reference triclinic phase reveals a slight but significant increase in overlap.

Quantifying the similarity of each crystallite to the two reference systems separates them into groups. Bulk HEX at 0.1 K/ps and HEX/Surf/water at 0.01 K/ps and 0.001 K/ps are in active transition to the triclinic phase. Bulk HEX at 0.1 K/ps is still in the early stages of the transition, while HEX/Surf/water at 0.01 K/ps is closest to the triclinic phase. The remaining crystallites remain very similar to the reference rotator phase.

**Table 15:** Jaccard indices calculated from the RDF profiles of each crystallite compared to those for the two reference systems.

System	Triclinic	R <sub>I</sub> → T
R <sub>I</sub> → T	0.34	1.00
<i>Bulk HEX</i>		
1 K/ps	0.35	0.82
0.1 K/ps	0.39	0.45
0.01 K/ps	0.30	0.72
0.001 K/ps	0.33	0.80
<i>HEX/Surf/water</i>		
1 K/ps	0.34	0.82
0.1 K/ps	0.34	0.76
0.01 K/ps	0.39	0.30
0.001 K/ps	0.39	0.51

#### 4.12.5. Analysis of the rotational freedom of the molecules

As already stated, a major distinction between rotator phases and the crystalline phase is the possibility of rotation of the molecules about their long axis, which can be determined by calculating the second principal axis (P<sub>2</sub>) of the molecules as described in Chapter 4.7. To quantify the rotational freedom, histograms of the angles between the P<sub>2</sub> of each molecule and the x-axis of the coordinate system are constructed. The values of P<sub>2</sub> are calculated for the entire studied time period (the last 100 ns of each MD trajectory). In a structure where all molecules are completely stationary, the result of the analysis will be a delta function centred at 0°. In a simulated crystal structure, the molecules are expected to oscillate slightly due to thermal motion, so the values will be slightly scattered around 0°. In contrast, crystallites in the rotator phase should have appreciably larger scattering.

To measure the dispersion of the angles, the central peaks of the histograms are fitted to a Gaussian function. The standard deviation of each fit is used as an indicator of the freedom of rotation. The values for all systems are presented in Table 16. All models, except HEX/Surf/water at 0.01 K/ps, have standard deviations close to those of the reference rotator phase. HEX/Surf/water at 0.01 K/ps appears very close to the triclinic phase. However, it is important to note that two satellite peaks are present in this system at ± 180°, suggesting that a large set of molecules has undergone a complete rotation about their long molecular axis in the 100 ns period.

This is an indication that the crystallite is in a period of active transition to a more ordered state. The reference triclinic phase profile, on the other hand, has only one intense peak centred at  $0^\circ$  and no satellite peak.

Bulk HEX at 0.1 K/ps also shows a nontrivial number of molecules rotating over the studied period (Figure 57, C). The  $\pm 80^\circ$  rotation and the main peak are characterized by the largest range of values, hence its relatively large standard deviation. These results, together with the other analyses summarized above, suggest that this system has high degree of ordering. However, it is in a state of active transition to another solid phase, which is best illustrated by the increased similarity of its RDF profile to the RDF profile of the triclinic reference system (Table 15).

**Table 16:** Standard deviations of the fitted Gaussian functions to the calculated histograms of the evolution of the angle between  $P_2$  and the  $x$ -axis of the coordinate system in the representative crystallites and in the reference systems.

System	Stand. deviation ( $^\circ$ )
<i>Triclinic crystal</i>	8
$R_I \rightarrow T$ layer 1	10.5
$R_I \rightarrow T$ layer 2	11
<i>Bulk HEX</i>	
1 K/ps	11
0.1 K/ps	13.5
0.01 K/ps	11.5
0.001 K/ps	11.5
<i>HEX/Surf/water</i>	
1 K/ps	11
0.1 K/ps	11
0.01 K/ps	7.5
0.001 K/ps	11

The remaining systems are very well described by their peak centred at  $0^\circ$  and a low-intensity satellite peak (Figure 57), similar to the profiles in the reference rotator phase (Figure 56, B).

The analyses presented so far clarify very well the degree of ordering in the model systems compared to the reference ones. Some of the systems are still in the initial stages of their transition to a fully ordered crystal structure, while others have advanced much further.

#### 4.12.6. Determining the phase state of the crystallites

It may be concluded from Table 3 that each rotator phase is uniquely distinguished by the combination of three parameters: the tilt angle of the molecules with respect to the crystallite plane ( $\theta$ ), the degree of deformation of the hexagonal lattice (D), and the azimuthal angle  $\Phi_d$ .

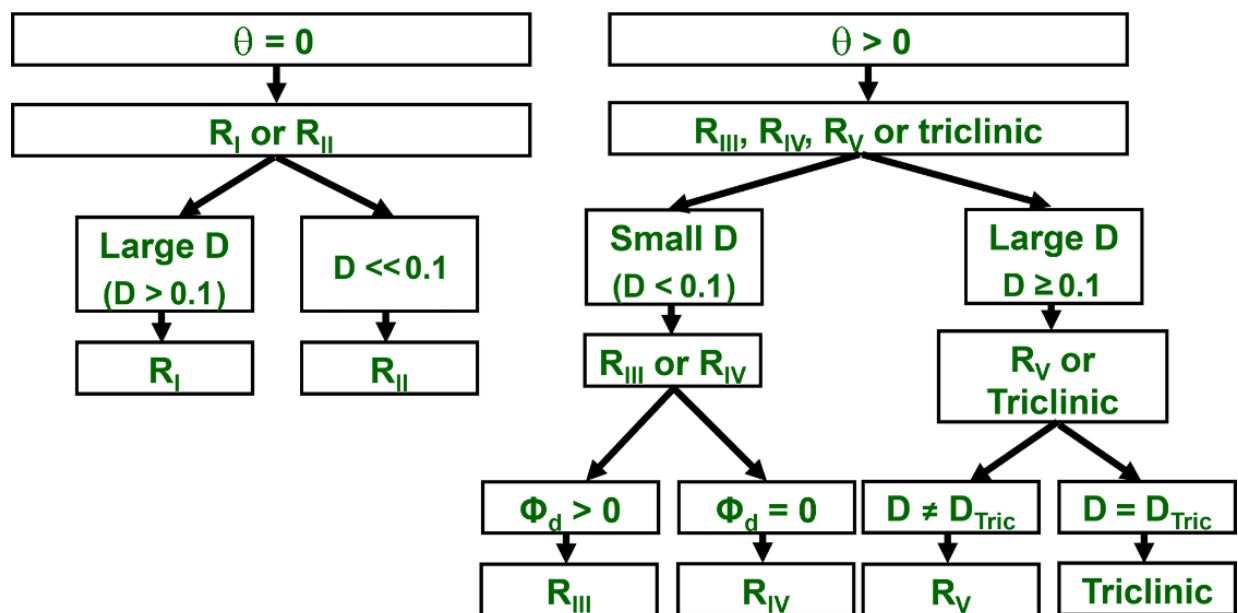


**Figure 58** Decision tree for determining the phase state of the studied crystallites based on  $\theta$ ,  $D$  and  $\Phi_d$ .  $R_x$  denotes the different rotator phases.

To determine the phase state of the crystallites, these three parameters are arranged hierarchically in a decision tree (Figure 58). First, the value of  $\theta$  is determined since this parameter can only be in two states:  $\theta = 0$  and  $\theta > 0$ . Then, it is evaluated whether  $D$  is 0, small or large. The limits of the values for small and large  $D$  are determined from the initial experimental structures of the reference triclinic crystal and the reference rotator phase, and these values are presented in Table 17. If  $\theta > 0$  and  $D \neq 0$ , then it is estimated if  $\Phi_d = 0$  or  $\Phi_d > 0$ . If  $D = 0$ , then  $\Phi_d$  cannot be calculated since the elementary cell is a regular hexagon. Last, if  $D$  is large, it is compared to the  $D$  of the triclinic phase, which is estimated to be 0.24 in the original triclinic crystal and  $\sim 0.29$  in the reference system after 1  $\mu$ s MD simulation.

The phase states of the two reference and of all simulated model systems are presented graphically in Figure 59. The triclinic phase remains almost unchanged throughout the simulation. The reference rotator phase is defined as  $R_{III}$ , although it was originally constructed as  $R_I$ . The transition from  $R_I$  to  $R_{III}$  begins almost instantaneously in the simulation with a tilt of the molecules at  $\sim 19^\circ$ , which is comparable to that in the triclinic phase, and  $D$  is relatively small. It is important to note that experimentally the  $R_I$  phase transitions directly to  $R_V$ , albeit for hydrocarbons with longer chains.<sup>5</sup> The question then arises why the simulations predict the initial HEX transition to be through  $R_{III}$ . This could be due to two reasons. It is possible that the transition to  $R_{III}$  takes place in a very short time interval, inaccessible to an experimental approach. The second reason may be the limited size of the model systems, which may favour the formation of a single-layer structure (AAAA) in the crystallites and, hence, the corresponding phase (Table 3). All spontaneously frozen model systems are indeed characterized by single-layered largest crystallites that have been analysed. However, the reference rotator phase is initially constructed as the  $R_I$

phase, which has a bilayer structure (ABAB, Figure 60, left). Therefore, the evolution of this structure during the 1  $\mu$ s simulation can be traced along the  $c$  direction of the lattice (Figure 60). It is evident that even at 500 ns the structure already approaches the AAAA type, as in the R<sub>III</sub> phase. This is maintained until the end of the simulation of the reference system. This indicates that the appearance of the R<sub>III</sub> phase is most likely a short-lived event.

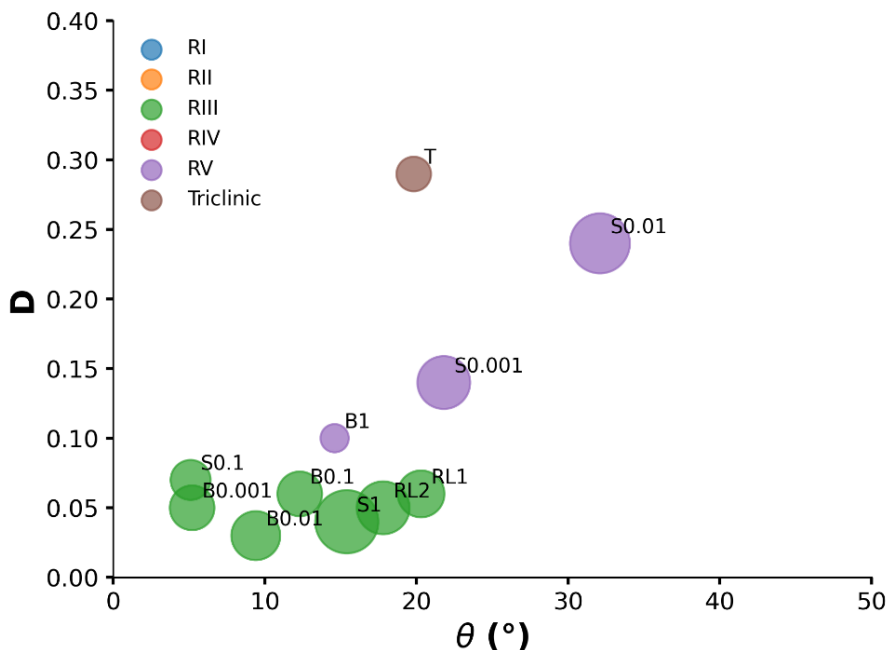


**Figure 59:** Graphical representation of the phase states of the reference systems and crystallites studied. "B" denotes bulk HEX, "S" denotes HEX/Surf/water, "RL1" and "RL2" denote rotator phase, layer 1 and layer 2, respectively, and "T" denotes triclinic phase. Each colour represents a different phase and the size of the circle reflects the magnitude of  $\Phi_d$ . The cooling rates are given as numerical indices.

Most of the crystallite parameters are comparable to those of the rotator phase R<sub>III</sub>. However, they can vary considerably, which is explained by the different stages of transition in the crystal evidenced by the other analyses discussed above. The crystallite from the HEX/Surf/water system at 0.01 K/ps is the one found to be in the most advanced transition from the R<sub>V</sub> to the triclinic state. The molecules in this crystallite have a very large  $\theta$  and a value for D that is close to that in the triclinic phase.  $\Phi_d > 0$ , which is not typical for R<sub>V</sub>. However, as indicated above, the crystallite undergoes an active transition from the solid state to the triclinic phase. There is another system characterized by an R<sub>V</sub>  $\rightarrow$  T transition (Figure 59, S0.001), but it is still at an earlier stage with respect to the deformation parameter D. Bulk HEX at 1 K/ps is the only crystallite in the R<sub>V</sub> phase.

The almost immediate transition of the reference rotator phase from R<sub>I</sub> to R<sub>III</sub> and most model systems in R<sub>III</sub> suggest that this is the possible phase in which hexadecane-containing

systems are organized. The overall classification of systems suggests that there may be several pathways for hexadecane crystallisation, such as: liquid  $\rightarrow$  R<sub>III</sub>  $\rightarrow$  R<sub>V</sub>  $\rightarrow$  triclinic, or liquid  $\rightarrow$  R<sub>V</sub>  $\rightarrow$  triclinic, or liquid  $\rightarrow$  R<sub>III</sub>  $\rightarrow$  triclinic.

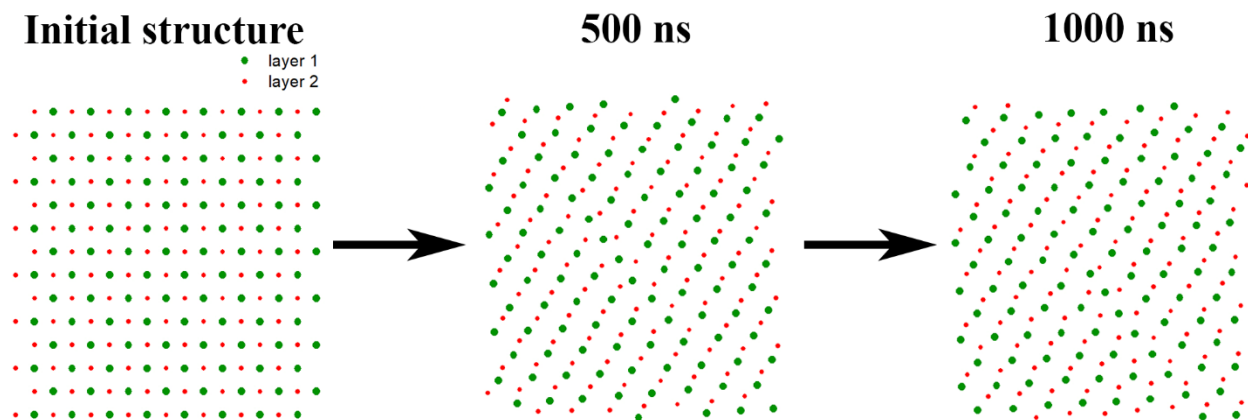


**Figure 60:** Evolution of the multilayer structure in the reference rotator phase (initially R<sub>I</sub>) over 1  $\mu$ s simulation time. Layer 1 is represented in green and layer 2 in red. The *c*-direction view of the lattice is given over the cross section of the alkyl chains with the *ab* plane.

Although R<sub>III</sub> has not been detected experimentally in hexadecane, it is important to note that the processes studied here are on the microsecond scale, with no bias in the simulations. It is evident that all systems studied, including the reference rotator phase, are in a state of transition and the observed phenomena are the initial stages of intermolecular organization leading eventually to a triclinic crystalline phase.

#### 4.13. Effect of the curvature on the freezing process of hexadecane

In order to investigate the effect of the curvature on the freezing process of hexadecane, a system of hexadecane, surfactant (C<sub>16</sub>EO<sub>2</sub>) and water is constructed. The organic fraction of the system is organized into a spherical droplet with a diameter of 15 nm, where the core is composed of hexadecane and the surfactant is located at the periphery of the droplet. The hexadecane molecules are placed in the initial configuration randomly using a Monte Carlo method until the experimental density of the oil is achieved.<sup>4</sup> The surfactant molecules are maximally packed at the surface of the droplet. The droplet is then solvated, with which the system consists of  $\sim$ 2 million atoms (Figure 61). Similar to the other systems investigated in the thesis, the force field CHARMM36 is used to describe the organic fraction and TIP4P – to describe the water.

As an initial step, the system is again heated to 350 K and then a production MD simulation is conducted at this temperature in NPT ensemble for 600 ns in order to reach equilibrium. The system is then cooled to 300 K and simulated again for 600 ns. The final structures obtained at the two temperatures are then used as the initial ones for cooling to 278 K. The two trajectories at 278 K are with 500 ns duration, which is sufficient to observe complete freezing in the droplet. A

comparison between the two final systems can elucidate the effect of the initial temperature from which freezing is initiated.

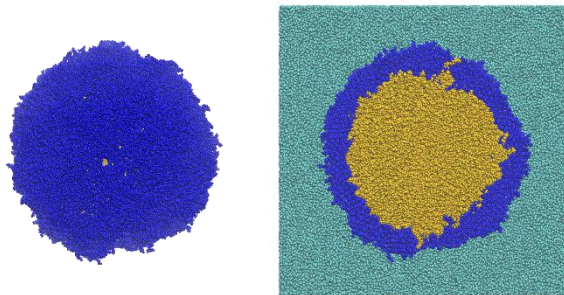


**Figure 61:** Initial configuration of the spherical drop containing hexadecane. The whole drop without water is shown on the left and a cross section of the system on the right.  $C_{16}EO_2$  is in blue, hexadecane in yellow and water in cyan.

The main difference between the two initial configurations (from 350 K and from 300 K) is the phase state of the surfactant molecules. At 350 K the whole system is in the liquid state (Figure 62, A), whereas at 300 K  $C_{16}EO_2$  is already frozen (Figure 62, B). When crystallization is initiated from 350 K,  $C_{16}EO_2$  and the hexadecane freeze simultaneously, whereas at 300 K the surface is already ordered and the crystallization process occurs only inside the droplet.

As shown in Figure 62, left, at 350 K the droplet remains spherical, while at 300 K a change in shape is initiated, which is characteristic of the formation of a rotator phase.<sup>5</sup> Since at 300 K freezing is observed only at the periphery of the droplet, this indicates that the change in shape is related to the surface freezing.

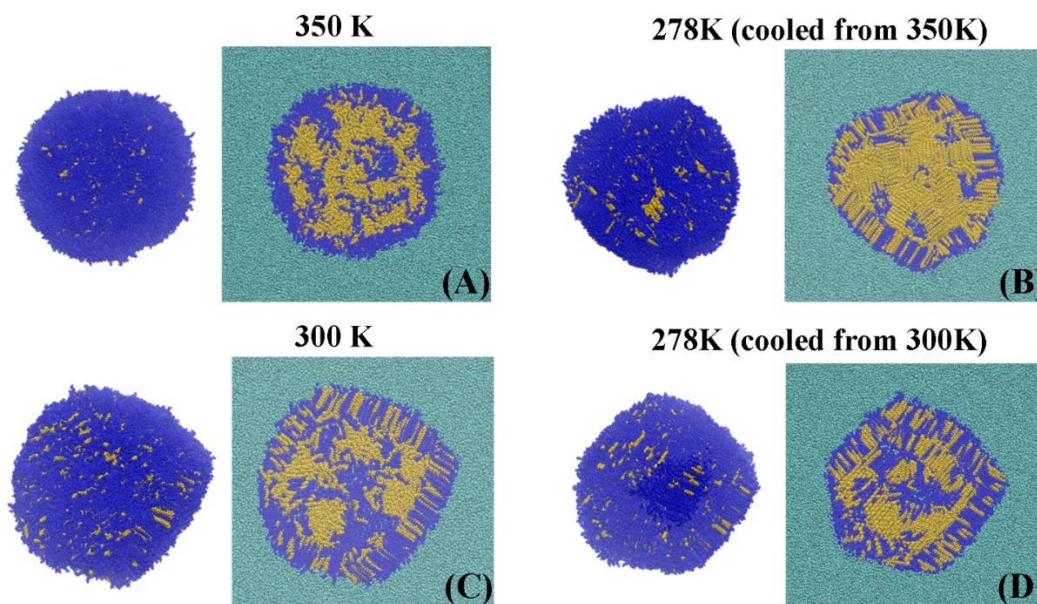


**Figure 62:** Final frames of the hexadecane/surfactant droplet at (A) 350 K, (B) 278 K cooled from 350 K, (C) 300 K, (D) 278 K cooled from 300 K; the same molecular representations are used as in Figure 61.

It may be seen from the final frames at 278 K (Figure 62, right) that the number of surfactant molecules on the surface when cooled from 350 K is significantly less than when cooled from 300 K. This is probably due to the still melted surfactant molecules at 350 K, which allows a more efficient redistribution of alkane and surfactant during freezing. This results in two different distributions of alkane and surfactant in the droplet, dependent on the initial temperature.

The shapes of the two drops at the end of the simulations are also different. When cooled from 300 K, the entire surface of the droplet is almost flat, in contrast to the system cooled from 350 K. The presence of these flat surfaces in the droplet is another indicator of the formation of a rotator phase.<sup>5</sup>

The described differences in the two systems allow the development of technological strategies to direct the alkane/surfactant droplets along different crystallization paths by varying the initial temperature before cooling.

## 5. Conclusions

The main objective of the thesis is to model and describe the freezing process of hexadecane-containing systems in which it is known that a transient rotator phase may exist.<sup>5</sup> Two types of models are built, one containing only hexadecane in the bulk (bulk HEX) and the other consisting of a hexadecane phase on a flat water surface stabilized by two surfactant layers (HEX/Surf/water). These two models are selected to evaluate the effect of the presence of surfactants in the system on the freezing process and the type of the obtained ordered phase.

The simulations are carried out using the molecular dynamics method, which is widely applied to study time-dependent processes.<sup>11,14,47,51,52</sup> The used force field is validated before performing the production simulations by requesting it to fulfil the following requirements: (i) after heating the system to 350 K, a phase transition from a regular lattice to an isotropic liquid should be observed; (ii) once the systems are in the isotropic liquid state, their bulk density should reproduce the experimental one or be close to it; (iii) freezing has to take place in the systems after cooling them to different temperatures between 273 K and 300 K. These three conditions are met by the CHARMM36 force field, which is then used to simulate all studied systems.

After the model systems are cooled to a temperature at which a phase transition from isotropic liquid to an ordered state (278 K) takes place, some key thermodynamic characteristics (enthalpy and density profiles) are investigated, and a large set of structural analyses are performed in order to assess the degree of ordering in the systems and to determine unambiguously the type of the obtained ordered phase. The effect of the cooling rate on the freezing process is also evaluated, which is why each model system is cooled at four different rates, 1 K/ps, 0.1 K/ps, 0.01 K/ps and 0.001 K/ps. In this way, the number of independent trajectories is also increased, which improves the statistical significance of the results. For all studied systems, the formation of a polycrystalline structure is observed but as the cooling rate decreases the number of molecules included in the largest crystallite increases.



Analysis of the crystal nuclei initially obtained in the systems shows two types of freezing. In bulk HEX, the molecules start to cluster in a random location in the system and they are in close proximity in space. This is indicative of homogeneous nucleation. On the other hand, in HEX/Surf/water, the surfactant surface serves as a template, so the molecules frozen initially are dispersed over the entire length of the crystallite. This is indicative of heterogeneous nucleation. These results are consistent with the known basics of crystallisation for these two types of systems.<sup>9</sup>

At the beginning of the freezing process, an abrupt change in enthalpy and density values is observed, which corresponds to the expected first-order phase transition from isotropic liquid to a solid phase. The enthalpy of the phase transition for each model system is compared with the experimental value for the transition from isotropic liquid to triclinic crystal of bulk hexadecane.<sup>5</sup> Five of the eight systems studied have transition enthalpies between 65% and 80% of that of the transition to the triclinic phase, an indication that they are in the rotator phase.<sup>5</sup> The remaining three systems (bulk HEX at 0.001 K/ps, HEX/Surf/water at 0.01 K/ps, and HEX/Surf/water at 0.001 K/ps) have a decrease in enthalpy above 80% of the experimental value, suggesting a more advanced stage of ordering towards a triclinic crystal.

Due to the polycrystalline nature of the investigated model systems, structural analyses cannot be performed directly on the generated trajectories, as different crystallites may have different degrees of ordering. For this purpose, a procedure is developed to isolate the crystallites and reconstruct their real-space coordinates, after which a representative crystallite is selected for each system and a detailed structural analysis is performed for it.

The radial distribution functions (RDFs) of the eight crystallites are calculated and compared with those of the two reference systems of bulk HEX in the rotator phase and in a triclinic crystal. The profiles of most systems overlap significantly with that of the reference rotator phase. Two of the crystallites (HEX/Surf/water at 0.01 K/ps and HEX/Surf/water at 0.001 K/ps) stand out with a significantly lower match to the rotator phase, confirming their advanced stage of transition.

The degree of conformational freedom in the studied crystallites is quantified by the number of *gauche* conformations in the crystallites, and the rotational freedom about the long axis of the molecules is quantified by the angle of the second principal axis ( $P_2$ ) of each molecule in the corresponding crystallite with the x axis of the coordinate system. The values obtained from the analysis of  $P_2$  correlate strongly with the percentage of *gauche* conformations in the torsion angles containing a methyl group. Bulk HEX at 0.1 K/ps has a larger number of *gauche* conformations and a larger standard deviation of  $P_2$  values relative to the reference rotator phase, indicating that the crystallite is in a state of active transition. On the other hand, the HEX/Surf/water crystallite at 0.01 K/ps has the smallest distribution of  $P_2$  values and the smallest number of *gauche* conformations, suggesting that this crystallite is in the most advanced stage of ordering. However, the presence of two satellite peaks in the  $P_2$  histogram confirms that the crystallite is still undergoing a phase transition to a triclinic crystal.

To determine the phase state of each of the studied crystallites, a combination of three structural parameters is calculated: the tilt angle of the molecules with respect to the crystallite plane ( $\theta$ ), the degree of deformation of the hexagonal lattice ( $D$ ) and the azimuthal angle ( $\Phi_d$ ). These parameters discriminate unequivocally between the five possible rotator phases and the triclinic crystal. However, their non-standard nature necessitates the development of procedures to estimate them, which is achieved in this thesis. Once numerical values for the three parameters are obtained, they are organized into a hierarchical structure in the form of a decision tree, where the final node defines the phase state of the corresponding crystallite.

Most of the crystallites studied are in the  $R_{III}$  phase, but the values of their structural parameters vary considerably. This is due to their different stage of transitioning to the triclinic crystal, which is confirmed by the other analyses carried out in the study. Two of the crystallites (HEX/Surf/water at 0.01 K/ps and HEX/Surf/water at 0.001 K/ps) are in the  $R_V \rightarrow T$  transition, and bulk HEX at 1 K/ps is the only crystallite in  $R_V$ . From these results, it may be suggested that several pathways are possible for freezing of hexadecane-containing systems to a triclinic crystal: liquid  $\rightarrow R_{III} \rightarrow R_V \rightarrow$  triclinic, liquid  $\rightarrow R_V \rightarrow$  triclinic, or liquid  $\rightarrow R_{III} \rightarrow$  triclinic. These two types of rotator phases are unusual for hexadecane from an experimental point of view but the study is focused on the initial freezing processes of these two models and such a short time interval is still inaccessible for experimental measurement.

A spherical drop of alkane/surfactant with a diameter of 15 nm is constructed and solvated in water. After cooling to 278 K from two initial temperatures (350 K and 300 K), significant differences in the crystallisation process are observed. It is concluded thereof that controlling the starting temperature before initiating the freezing process influences the crystallisation pathway.

So far, the study of ordered phases in alkane-containing systems has usually been conducted by constructing a model system in a predefined phase state.<sup>11,14</sup> This approach allows shorter simulations to obtain meaningful results, thus reducing computational time. However, it can introduce bias in the simulations. Also, the phase state of the systems is described by one or two structural parameters. For example, Wentzel et al. define parameters similar to those of Ising and Potts to distinguish the phases  $R_I$  and  $R_{II}$ .<sup>11</sup> Ryckaert et al. monitor the tilt of the molecules with respect to the crystal plane and the rotational disorder in the crystal.<sup>14</sup> This approach has two major drawbacks. The information from these analyses is not sufficient to distinguish all possible rotator phases. Also, the analyses depend on the orientation of the crystal in the coordinate system. The computational protocol used in the thesis allows systems to transition freely from solid to liquid state upon heating of the system and vice versa upon cooling. The developed structural analyses are independent of the coordinate system, allowing the assessment of the properties of polycrystalline structures. The combination of the three structural parameters discriminates between all five possible rotator phases and the triclinic crystal.

## 6. Contributions

The following scientific contributions can be formulated as a result of the work on the PhD thesis:

1. A new computational protocol is proposed for conducting classical atomistic molecular dynamics (MD) simulations of hexadecane-containing systems, in which transitions from a regular lattice of hexadecane to an isotropic liquid (melting) and from an isotropic liquid to an ordered state (freezing) are successfully reproduced.

2. The freezing mechanism of bulk hexadecane and of hexadecane in contact with water at an interface stabilised by a long-chain surfactant is investigated at the molecular level using the proposed protocol. In the freezing process, the formation of intermediate, polycrystalline rotator phases are observed, which is in agreement with experimental data of other authors.

3. A set of specialised procedures is developed for the structural analysis of polycrystalline model systems composed of quasilinear molecules.

4. Structural analysis of the hexadecane crystallites in the frozen model systems is performed using the developed procedures. The type of solid phases is identified and possible sequences of intermediate phase transitions during hexadecane crystallisation are proposed.

### **List of publications that have emerged from the work on the thesis:**

**1. Computational assessment of hexadecane freezing by equilibrium atomistic molecular dynamics simulations**

Stoyan Iliev, Sonya Tsibranska, Anela Ivanova, Slavka Tcholakova, Nikolai Denkov  
*Journal of Colloid and Interface Science* **2023**, 638, 743-757, IF: 9.9, Q1, citations: 6  
DOI: 10.1016/j.jcis.2023.01.126

**2. Computational Procedure for Analysis of Crystallites in Polycrystalline Solids of Quasilinear Molecules**

Stoyan Iliev, Sonya Tsibranska, Ilija Kichev, Slavka Tcholakova, Nikolai Denkov, Anela Ivanova  
*Molecules* **2023**, 28, 2327, IF: 4.6, Q1, citations: 0  
DOI: 10.3390/molecules28052327

**3. Types of phases obtained by molecular dynamics simulations upon freezing of hexadecane-containing systems**

Sonya Tsibranska, Stoyan Iliev, Anela Ivanova, Nikola Aleksandrov, Slavka Tcholakova, Nikolai Denkov  
*Colloids and Surfaces A: Physicochemical and Engineering Aspects* **2024**, 697, 134466, IF: 5.2, Q1, citations: 0  
DOI: 10.1016/j.colsurfa.2024.134466

### **Presentation of the results at scientific conferences:**

- 1. XIX National Conference of Chemistry for Undergraduates and PhD Students, 2-4 June, 2021, Sofia, Bulgaria**  
Modeling of hexadecane crystallisation in bulk and at an interface with molecular dynamics  
Iliev, S., Tsibranska, S., Ivanova, A., Cholakova, S., Denkov, N.  
(oral presentation)
- 2. Bunsen-Tagung, 10-12 May, 2021, online**  
Modelling rotator phases of alkane-containing systems  
Iliev, S., Ivanova, A., Tsibranska, S., Tcholakova, S., Denkov, N.  
(poster)
- 3. XX National Conference of Chemistry for Undergraduates and PhD Students, 18-20 May, 2022, Sofia, Bulgaria**  
Identification and analysis of ordered structures in hexadecane-containing systems modelled with molecular dynamics  
Iliev, S., Tsibranska, S., Ivanova, A., Cholakova, S., Denkov, N.  
(oral presentation)
- 4. 11<sup>th</sup> International Colloids Conference, 12-15 June, 2022, Lisbon, Portugal**  
Monitoring freezing at surfactant-stabilized hexadecane/water interface by molecular dynamics - effect of surface curvature  
Tsibranska, S., Iliev, S., Ivanova, A., Tcholakova, S., Denkov, N.  
(oral presentation)
- 5. Psi-K Conference, 22-25 August, 2022, Lausanne, Switzerland**  
Structural analysis of ordered phases in hexadecane-containing systems obtained by molecular dynamics  
Iliev, S., Ivanova, A., Tsibranska, S., Tcholakova, S., Denkov, N.  
(poster)
- 6. 36<sup>th</sup> European Colloid & Interface Society Conference, 4-9 September, 2022, Chania, Crete, Greece**  
Monitoring freezing at surfactant-stabilized hexadecane/water interface by molecular dynamics  
Tsibranska, S., Iliev, S., Ivanova, A., Tcholakova, S., Denkov, N.  
(oral presentation)
- 7. XXII National Conference of Chemistry for Undergraduates and PhD Students, May 15-17, 2024, Sofia, Bulgaria**  
Determination of phases obtained from molecular dynamics simulations of hexadecane-containing systems after freezing  
Iliev, S., Tsibranska, S., Ivanova, A., Alexandrov, N., A., Cholakova, S., Denkov, N.  
(oral presentation)

## 7. References

---

- <sup>1</sup> D. M. Small, "The Physical Chemistry of Lipids: from Alkanes to Phospholipids" *Plenum Press, New York* (1986).
- <sup>2</sup> E. B. Sirota, D. M. Singer, "Phase transitions among the rotator phases of the normal alkanes" *J. Chem. Phys.* **101** (1994) 10873.
- <sup>3</sup> E. B. Sirota, A. B. Herhold, "Transient Phase-Induced Nucleation" *Science* **283** (1999) 529-532.
- <sup>4</sup> J. H. Dymond, K. R. Harris, "The temperature and density dependence of the self-diffusion coefficient of n-hexadecane," *Mol. Phys.* **75** (1992) 461-6.
- <sup>5</sup> D. Cholakova, N. Denkov. "Rotator phases in alkane systems.
- <sup>6</sup> J. H. Hildebrand, "Motions of molecules in liquids: viscosity and diffusivity" *Science* **171** (1971) 490-3.
- <sup>7</sup> M. J. Oliver, P. D. Calvert, "Homogeneous nucleation of n-alkanes measured by differential scanning calorimetry" *J. Cryst. Growth* **30** (1975) 343-51.
- <sup>8</sup> D. R. Uhlmann, G. Kritchevsky, R. Straff, G. Scherer, "Crystal nucleation in normal alkane liquids" *J. Chem. Phys.* **62** (1975) 4896-903.
- <sup>9</sup> E. Mura, Y. Ding, "Nucleation of melt: From fundamentals to dispersed systems" *Adv. Colloid Interf. Sci.* **289** (2021) 102361.
- <sup>10</sup> Д. Cholakova, "Spontaneous Deformations of Emulsion Drops Undergoing Phase Transition", PhD Thesis, St. Kliment Ohridski", Faculty of Chemistry and Pharmacy, 2020.
- <sup>11</sup> N. Wentzel, T. S. Milner "Simulation of multiple ordered phases in C23 n-alkane" *J. Chem. Phys.* **134** (2011) 224504.
- <sup>12</sup> D. J. Tobias, K. Tu, M. L. Klein, "Assessment of all-atom potentials for modeling membranes: molecular dynamics simulations of solid and liquid alkanes and crystals of phospholipid fragments," *J. Phys. Chem. Chim. Phys. Phys.-Chim. Biol.* **94** (1997) 1482-502.
- <sup>13</sup> A. Marbeuf, R. Brown "Molecular dynamics in n-alkanes: Premelting phenomena and rotator phases" *J. Chem. Phys.* **124** (2006) 054901.
- <sup>14</sup> Ryckaert, J.-P.; McDonald, I.; Klein, M. Disorder in the pseudohexagonal rotator phase of n-alkanes: molecular-dynamics calculations for tricosane, *Mol. Phys.* **67** (1989) 957-979.
- <sup>15</sup> Klauda, J.; Venable, R.; Freites, J.; O'Connor, J.; Tobias, D.; Mondragon-Ramirez, C.; Vorobyov, I.; MacKerell, Jr. Update of the CHARMM All-atom additive force field for lipids: validation on six lipid types. *J. Phys. Chem. B* **2010**, *114*, 7830-7843.
- <sup>16</sup> Siu, S. W. I.; Pluhackova, K.; Böckmann, R. A. Optimization of the OPLS-AA force field for long hydrocarbons. *J. Chem. Theory Comput.* **2012**, *8*, 1459-1470.
- <sup>17</sup> S. A. Burrows, I. Korotkin, S. K. Smoukov, E. Boek, and S. Karabasov, "Benchmarking of molecular dynamics force fields for solid-liquid and solid-solid phase transitions in alkanes," *J. Phys. Chem. Phys. Chem. B* **125** (2021) 5145-59.
- <sup>18</sup> S. Gamisch, M. Kick, F. Klünder, J. Weiss, E. Laurenz, T. Haussmann "Thermal Storage.
- <sup>19</sup> Jorgensen, W.; Madura, J. Temperature and size dependence for Monte Carlo simulations of TIP4P water. *Mol. Phys.* **1985**, *56*, 1381-1392.
- <sup>20</sup> Iliev, S.; Kichev, I.; Tsibranska, S.; Ivanova, A.; Tcholakova, S.; Denkov N. Computational procedure for analysis of crystallites in polycrystalline solids of quasilinear molecules, *Molecules.* **28** (2023) 2327.
- <sup>21</sup> G. Bussi, D. Donadio, and M. Parrinello, "Canonical sampling through velocity rescaling," *J. Chem. Phys.*, **126** (2007) 014101.

- 
- <sup>22</sup> Berendsen, H.J., Postma, J.V., Van Gunsteren, W.F., DiNola, A.R.H.J. and Haak, J.R., Molecular dynamics with coupling to an external bath. *J. Chem. Phys.*, **81** (1984) 3684-3690.
- <sup>23</sup> Tardajos, G.; Diaz Peña, M.; Aicart, E. Velocity of sound in pure liquids by a pulse-echo-overlap method. *J. Chem. Thermodyn.* **1986**, *18*, 683-689.
- <sup>24</sup> Parrinello, M.; Rahman, A. *J. Appl. Phys.* **1981**, *52*, 7182-7190.
- <sup>25</sup> Frenkel, D.; Smit, B. Understanding Molecular Simulation, Academic Press: San Diego, **2002**.
- <sup>26</sup> T. Darden, D. York, and L. Pedersen, "Particle mesh Ewald. *Chem. Phys.*, **98** (1993) 10089-10092.
- <sup>27</sup> B. Hess, H. Bekker, H.J.C. Berendsen, and J.G.E.M. Fraaije, "LINCS: A linear constraint solver for molecular simulations," *J. Comp. Chem.*, **18** (1997) 1463-1472 (1997).
- <sup>28</sup> S. Miyamoto and P.A. Kollman, "SETTLE: An analytical version of the SHAKE and RATTLE algorithms for rigid water models," *J. Comp. Chem.*, **13** (1992) 952-962.
- <sup>29</sup> (a) Dickson, C. J.; Madej, B. D.; Skjerve, Å. A.; Betz, R. M.; Teigen, K.; Gould, I. R.; Walker, R. C. Lipid14: The Amber Lipid Force Field. *J. Chem. Theory Comput.* **2014**, *10*, 865-879; (b) Madej, B.; Gould, I.; Walker, R. A parameterization of cholesterol for mixed lipid bilayer simulation within the Amber Lipid14 force field *J. Chem. Phys. Chem. B* **2015**, *119*, 12424-12435. doi: 10.1021/acs.jpcc.5b04924.
- <sup>30</sup> Cornell, W.; Cieplak, P.; Bayly, C.; Gould, I.; Merz, K.; Ferguson, D.; Spellmeyer, D.; Fox, T.; Caldwell, J.; Kollman, P. A second-generation force field for the simulation of proteins, nucleic acids, and organic molecules. *J. of Am. Chem. Soc.* **1995**, *117*, 5179-5197. doi: 10.1021/ja00124a002.
- <sup>31</sup> Abraham, M.; Murtola, T.; Schulz, R.; Páll, S.; Smith, J.; Hess, B.; Lindahl, E. GROMACS: High performance molecular simulations through multi-level parallelism from laptops to supercomputers. *Software X* **2015**, *1-2*, 19-25. doi: 10.1016/j.softx.2015.06.001.
- <sup>32</sup> Humphrey, W.; Dalke, A.; Schulten, K. VMD: Visual molecular dynamics. *J. Mol. Graph.* **1996**, *14*, 33-38. doi: 10.1016/0263-7855(96)00018-5.
- <sup>33</sup> (a) Gowers, R.J.; Linke, M.; Barnoud, J.; Reddy, T.J.E.; Melo, M. N.; Seyler, S. L.; Dotson, D. L.; Domanski, J.; Buchoux, S.; Kenney, I. M.; Beckstein, O. MDAAnalysis: A Python package for the rapid analysis of molecular dynamics simulations. In S. Benthall and S. Rostrup (Eds.) *Proceedings of the 15<sup>th</sup> Python in Science Conference*, pages 98-105, Austin, USA, **2016**, SciPy, doi:10.25080/majora-629e541a-00e.
- (b) Michaud-Agrawal, N.; Denning, E. J.; Woolf, T. B.; Beckstein, O. MDAAnalysis: A Toolkit for the Analysis of Molecular Dynamics Simulations. *J. Molecular Dynamics. Comput. Chem.* **2011**, *32*, 2319-2327, doi:10.1002/jcc.21787. PMID:PMC3144279
- <sup>34</sup> Harris, C.R.; Millman, K.J.; van der Walt, S.J.; Gommers, R.; Virtanen, P.; Cournapeau, D.; Wieser, E.; Taylor, J.; Berg, S.; Smith, N. J.; Kern, R.; Picus, M.; Hoyer, S.; van Kerkwijk, M. H.; Brett, M.; Haldane, A.; Fernández del Río, J.; Wiebe, M.; Peterson, P.; Gérard-Marchant, P.; Sheppard, K.; Reddy, T.; Weckesser, W.; Abbasi, H.; Gohlke, Ch.; Oliphant, T. E. Array programming with NumPy. *Nature* **2020**, *585*, 357-362. DOI: 10.1038/s41586-020-2649-2.
- <sup>35</sup> Hunter, J. D. Matplotlib: A 2D Graphics Environment. *Comput. Sci. Eng.* **2007**, *9*, 90-95. doi: 10.1109/MCSE.2007.55
- <sup>36</sup> Pearson, K. F.R.S. LIII. On lines and planes of closest fit to systems of points in space. *The London, Edinburgh, and Dublin Philosophical Magazine and Journal of Science.* **1901**, *2*, 559-72.
- <sup>37</sup> Pearson, K. F.R.S. LIII. On lines and planes of closest fit to systems of points in space. *Lond. Edinb. Dublin philos mag.* **2** (1901) 559-72

- 
- <sup>38</sup> Aurenhammer, F. Voronoi Diagrams - A survey of a fundamental geometric data structure. *ACM Comput. Surv.* **23** (1991) 345-405.
- <sup>39</sup> Okabe, A.; Boots, B.; Sugihara, K.; Chiu, S.; Kendall, D. Spatial Tessellations: Concepts and Applications of Voronoi Diagrams, 2nd ed.; Wiley: New York, **2000**. ISBN: 978-0-471-98635-5.
- <sup>40</sup> Gibbs, J. W.; Wilson, E. B. Vector Analysis. Willard Gibbs. Nabu Press: New York, Dover, **1960**.
- <sup>41</sup> (a) Dickson, C. J.; Madej, B. D.; Skjevik, Å. A.; Betz, R. M.; Teigen, K.; Gould, I. R.; Walker, R. C. Lipid14: The Amber Lipid Force Field. *J. Chem. Theory Comput.* **2014**, *10*, 865-879; (b) Madej, B.; Gould, I.; Walker, R. A parameterization of cholesterol for mixed lipid bilayer simulation within the Amber Lipid14 force field *J. Chem. Phys. Chem. B* **2015**, *119*, 12424-12435. doi: 10.1021/acs.jpcc.5b04924.
- <sup>42</sup> Cornell, W.; Cieplak, P.; Bayly, C.; Gould, I.; Merz, K.; Ferguson, D.; Spellmeyer, D.; Fox, T.; Caldwell, J.; Kollman, P. A second-generation force field for the simulation of proteins, nucleic acids, and organic molecules. *J. of Am. Chem. Soc.* **1995**, *117*, 5179-5197. doi: 10.1021/ja00124a002.
- <sup>43</sup> Outcalt, S.; Laesecke, A.; Fortin, T. J.. Density and speed of sound measurements of hexadecane. *J. Chem. Thermodyn.* **2010**, *42*, 700-706.
- <sup>44</sup> Denkov, N.; Tcholakova, S.; Lesov, I.; Cholakova, D.; Smoukov, S. Self-shaping of oil droplets via the formation of intermediate rotator phases upon cooling. *Nature* **2015**, *528*, 392-395.
- <sup>45</sup> Esselink, K.; Hilbers, P.; van Beest, B. Molecular dynamics study of nucleation and melting of n-alkanes, *J. Chem. Phys.* **1994**, *101*, 9033-9041.
- <sup>46</sup> Z. Rao, S. Wang, F. Peng "Self diffusion and heat capacity of n-alkanes based phase change materials: A molecular dynamics study" *Int. J. Heat Mass Transf.* **64** (2013) 581-9.
- <sup>47</sup> Y. Tsuchiya, H. Hasegawa, T. Iwatsubo, "Prediction of the melting point of n-alkanes using the molecular dynamics method" *J. Chem. Phys.* **114** (2001) 2484-8.
- <sup>48</sup> Craig, S.; Hastie, G.; Roberts, K.; Sherwood, J. Investigation into the structures of some normal alkanes within the homologous series C<sub>1328</sub>H<sub>28</sub> to C<sub>60122</sub>H<sub>122</sub> using high-resolution synchrotron X-ray powder diffraction. *J. Mat. Chem.* **1994**, *4*, 977-981.
- <sup>49</sup> Hegger, R.; Kantz, H.; Schreiber, T. Practical implementation of nonlinear time series methods: The TISEAN package. *CHAOS* **1999**, *9*, 413-435.
- <sup>50</sup> Jaccard, P. Nouvelles recherches sur la distribution florale. *Bull. Soc. Vaud. Sci. Nat.*, **1908**, *44*, 223-70.
- <sup>51</sup> N. Wentzel, T. S. Milner. "Crystal and rotator phases of n-alkanes: A molecular dynamics study" *J. Chem. Phys.* **132** (2010) 044901.
- <sup>52</sup> Y. Tsuchiya, H. Hasegawa, T. Iwatsubo, "Prediction of the latent heat of n-alkanes using the molecular dynamics method" *J. Appl. Phys.* **42** (2003) 6508.